Final Technical Report
June 2010

Calibration of Absolute Ground Motion Scaling for the Central Mississippi Valley using ANSS Digital Data

USGS Grant 06HQGR0110

Robert B. Herrmann
Department of Earth and Atmospheric Sciences
Saint Louis University
3642 Lindell Boulevard, O'Neil Hall
St. Louis, MO 63108

TEL: 314-977-3120, FAX 314-977-3117, Email rbh@eas.slu.edu

Final Technical Report
June 2010

Calibration of Absolute Ground Motion Scaling for the Central Mississippi Valley using ANSS Digital Data

USGS Grant 06HQGR0110

Robert B. Herrmann
Department of Earth and Atmospheric Sciences
Saint Louis University
3642 Lindell Boulevard, O'Neil Hall
St. Louis, MO 63108

TEL: 314-977-3120, FAX 314-977-3117, Email rbh@eas.slu.edu

Key words: Seismology, high frequency ground motion, New Madrid, Southeast Canada

Abstract

This effort focuses on assembling an extensive data set of digital recordings of small earthquakes that occurred and were recorded in southeastern Canada and the New Madrid region of the central United States. A data set of over 15000 waveforms was assembled for this comparison. Rather than develop a new ground motion scaling model, the data sets are compared to the Atkinson and Boore (1995) and Atkinson (2004) models for eastern North America. Using moment magnitudes determined under current and previous USGS support, these models can be evaluated in an absolute sense. The Atkinson and Boore (1995) model is preferred for southeastern Canada. For the New Madrid region neither characterizes derived ground motion scaling with distance, although the Atkinson and Boore (1995) does better in predictin g the scaling of motions with earthquake moment magnitude.

1. Comparisons of the Southeastern Canada and New Madrid Data sets

This report consists of three sections and an Appendix: A summary comparison of the regression results from the data sets followed by a detailed discussion of the New Madrid and Southeastern Canada data sets.

For the central U. S., the data sets were generated by the seismic networks sponsored by the USGS and USNRC and operated by Saing Louis University and CERI at the University of Memphis. The central U. S. data set was assembled by Mohammed Samiezade-Yazd, Luca Malagnini and Julia Kurpan during their tenure at Saint Louis University. The southeastern Canada data set was put together by

Young-Soo Jeon as part of his doctoral studies at Saint Louis University.

Regression and Modeling

As discussed in Sections 2 and 3, we work with ground velocity waveforms in units of m/s. These waveforms are then narrow band-pass filtered at selected center frequencies and peak motion associated with the S-wave arrive is determined. We also define a duration of the S-wave arrival, and use that duration to define a window for estimating the Fourier velocity spectra for a given trace. Rather than fitting the observed data to a specific model, we apply a two-step process: first let the data define an empirical ground motion model, and second, find a forward model that matches the regression model.

Since our objective is to find a forward model that fits all observations, we apply a regression to the peak velocity and Fourier velocity spectra at each center frequency. We also reguire that a forward model connect the two data sets through the duration in the context of random vibration theory.

The regression model is of the form

$$A = E + S + D \qquad (1)$$

where A is the logarithm of the peak motion or Fourier velocity, E is an excitation term, and D is a distance dependent term and S is a site/component modification term.. The overriding concern here is to have the regression model interpolate rather than extrapolate the observed data. Thus we define E as the expected level of motion at a distance where there are data. D is a term that propagates that expected value to the desired distance, and S modifies that motion for a given site. Although this equation has the correct physics, direct application is unstable unless constraints are applied. We require the $D(r_{ref}) = 0$ at the reference distance, which we take a 40 km for both data sets, that D(r) be smooth, and that $\Sigma S = 0$ is some manner. The site term could be constrained by reference to a common site, but we choose to force the ΣS(vertical component) = 0. These empirical terms can be interpreted in terms of a forward model:

$$a(r, f) = s(f, \mathbf{M}_W) g(r) e^{-\pi f r / Q(f) \beta} V(f) e^{-\pi f \kappa} \quad (2)$$

where $a(r, f)$ is the Fourier velocity spectra, $s(f, \mathbf{M}_W)$ is the source excitation as a function of moment-magnitude, $g(r)$ is the geometrical spreading function, $Q(f)$ is the frequency dependent quality factor which equals $Q_0(f/1.0)^{\eta}$, Q_0 is the quality factor at 1.0 Hz, $V(f)$ is a frequency dependent site amplification, and κ controls site dependent attenuation of high frequency. The $s(f, \mathbf{M}_W)$ here contains the effects of free surface partition of amplitude, the average source radiation pattern as well as source spectral scaling.

A comparison of the regression parameters for the Velocity spectra to the terms of this formula shows the association:

$$10^E = s(f, \mathbf{M}_W) g(r_{ref}) e^{-\pi f r_{ref} / Q(f) \beta} \overline{V(f)} e^{-\pi f \bar{\kappa}} \quad (3)$$

$$10^D = \frac{g(r) e^{-\pi f r / Q(f) \beta}}{g(r_{ref}) e^{-\pi f r_{ref} / Q(f) \beta}} \quad (4)$$

$$10^{S_i} = \frac{V(f) e^{-\pi f \kappa}}{\overline{V(f) e^{-\pi f \kappa}}}, \quad (5)$$

where $\overline{V(f) e^{-\pi \kappa f}}$ is the network average site effect arising from the site-term constraint.

This interpretation is consistent with the text above discussing each term. We consider two models that have been proposed for eastern North America: Atkinson and Boore (1995), denoted as AB95, and Atkinson (2004), denoted as A2004. The AB95 model provides sufficient detail to characterize all terms in equations 2- 4. The A2004 model does not discuss the source scaling in a manner that we can use, so we use a Brune model with 200 bar stress drop. We use our modifications of the SMSIM package to make predictions of the spectra and peak filtered gound velocities. These programs use the model specification files given in the Appendix of this report.

Distance Dependence – D(r)

We first compare the D(r) derived from the regression analysis to that predicted by the two models. Rather than plotting the D(r), we plot a deviation from 1/r spreading, e.g., D(r) + log (r/40) in Figure 1.1 for the Fourier velocity spectra and Figure 1.2 for the peak filtered velocity.

These figures indicate that there are significant differences in the observed distance dependence for the two study regions. The New Madrid motions are higher between 40 and about 150 km, and very much so between 150 and 400 km. This can be interepreted as the effect of different Q(f) and effective geometrical spreading.

For southeastern Canada, the AB95 model does better in fitting the D(r) than the A2004 (Fig. 3.5 and 3.6) for the Fourier velocity spectra. Neither do well in fitting the D(r) for the New Madrid data set (Figures 2.5, 2.6, 2.12 and 2.13).

Thus the ground motion scaling with distance for southeastern Canada cannot be applied to New Madrid and neighboring regions in the central U.S.

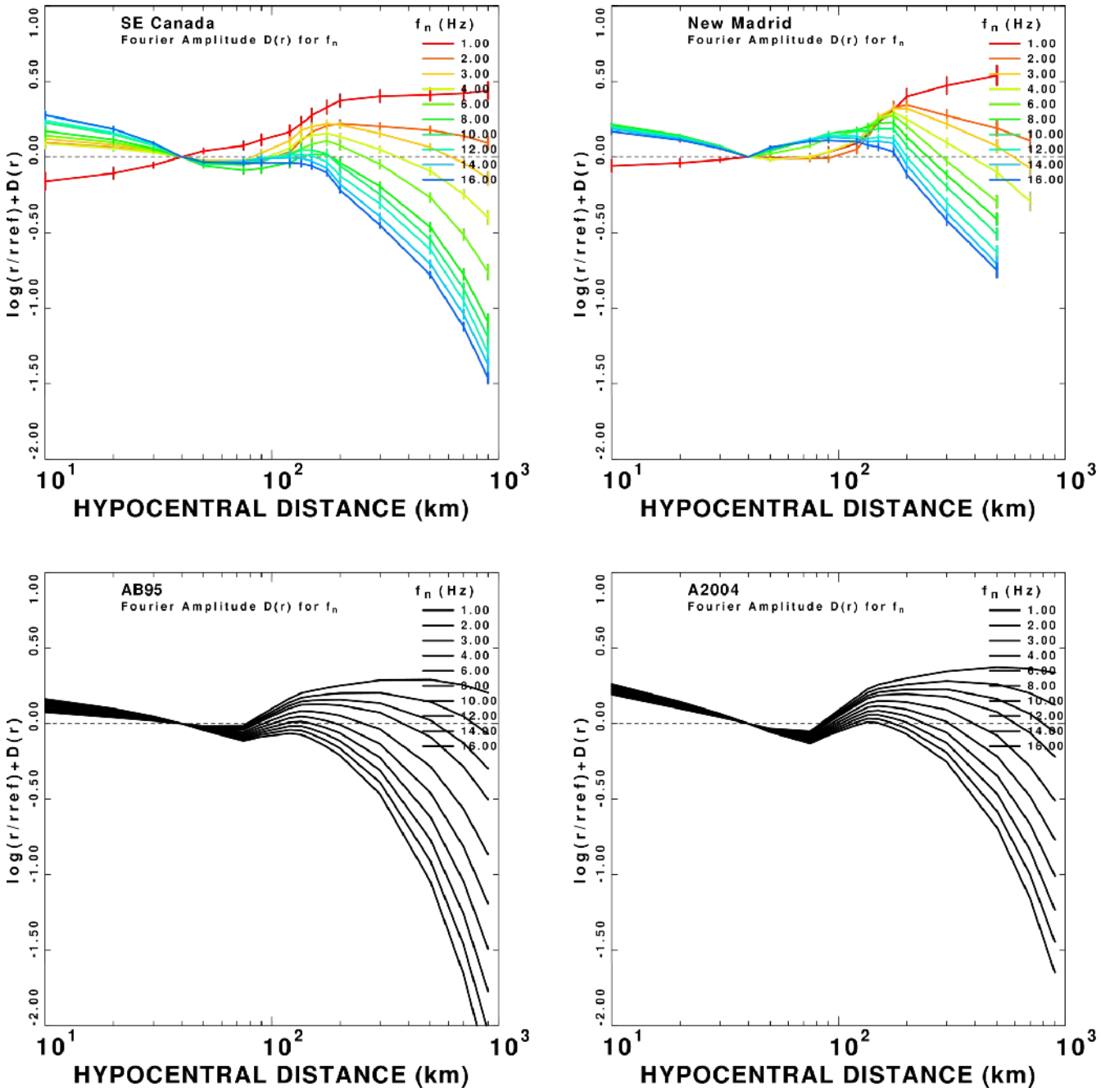

Fig. 1.1. Comparison of the D(r) + log(r/40) term for Fourier velocity spectra for the observed data (color) and model predictions (black).

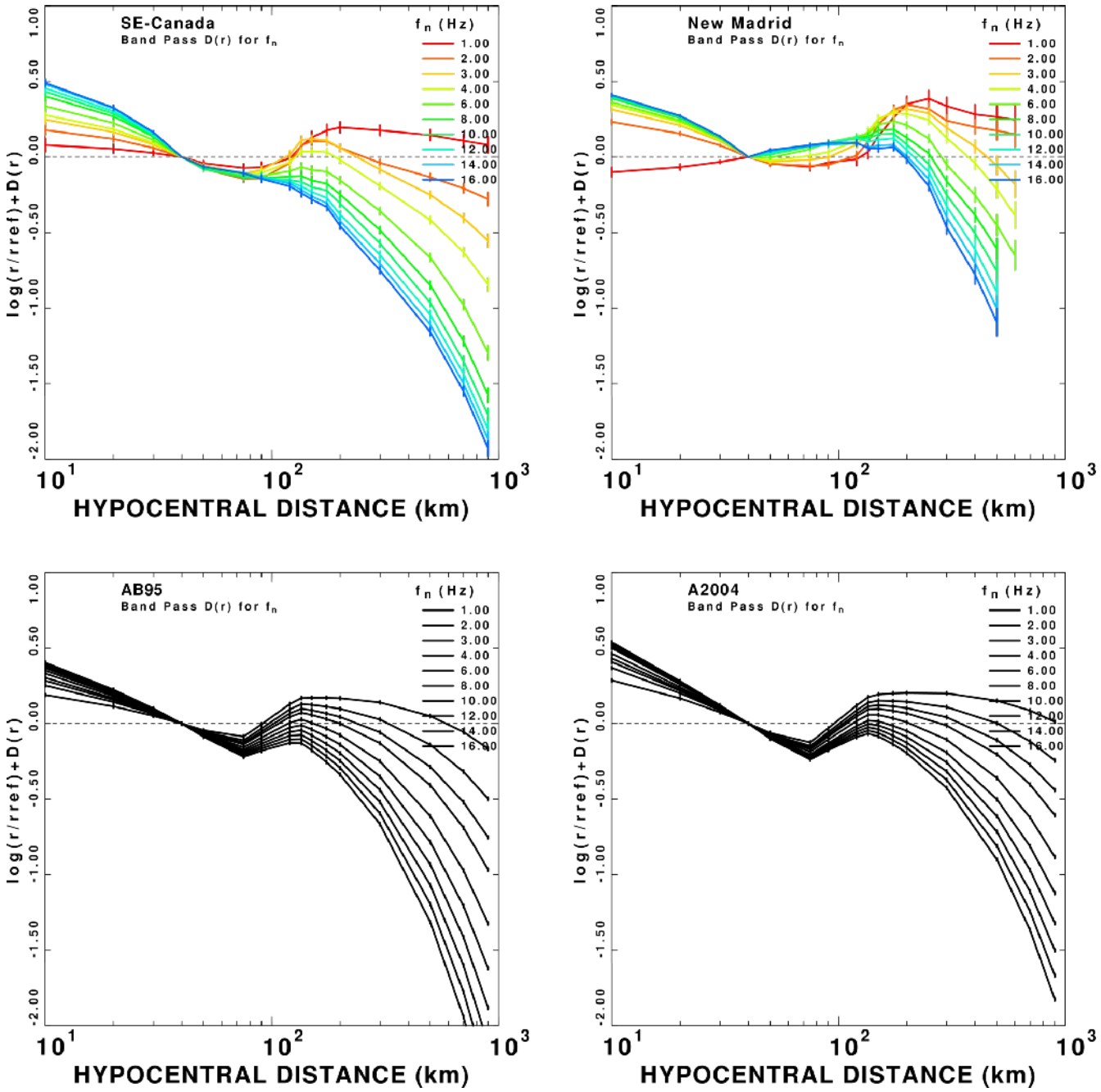

Fig. 1.2. Comparison of the D(r) + log(r/40) term for peak filtered velocity for the observed data (color) and model predictions (black).

We also compared the regression excitation terms, E(f), to the two model predictions, in Figures 2.9 and 2.16 for New Madrid and 3.9 and 3.15 for Southeastern Canada. For both regions, the model predicted excitations of E(r) at 40 km from the source show that the A2004 model underestimates the values derived from the regression.

We find different H/Z ratios for the two study regions (Figures 2.10 and 2.17 for New Madrid vs Figures 3.10 and 3.16 for Southeastern Canada). This is not surprising since the predominance of waveforms for the New Madrid study were from the deep sediment sites of the central Mississippi Valley. The strong sediment effect affects the meaning of the E(f), which for our constraints, represents the expected network averaged vertical component ground motion at 40 km from the source. What is the site amplification of the vertical component. We know that this should consist of a term such as

$$V(f) \exp (- \pi\kappa f)$$

Since previoous work has show that the vertical component motion associated with the S-arrival is the result of an S → P conversion at the rock – sediment interface at depth, we believe that the V(f) term will no be as strongly frequency dependent for the vertical component as for the horizontal components since one will use the P-wave velocity of about 1500 m/s instead of the S-wave velocity of about 300 m/s in the impedance relation used to determine V(f).

We have not considered the determination of the kappa value, although the data are sufficient. We have also not included sufficient data from 3-component stations outside the embayment for further insight on the site term.

The data strong ly suggest that the AB95 model is preferred over the A2004 model as interpreted by us.

2. High Frequency Ground motion Data Set for the Central Mississippi Valley

Introduction

This document describes a data set derived from digital recordings of earthquakes in the seismic zones surrounding New Madrid, Missouri. The data set consists of 632 earthquakes from March 13, 1980 to June 5, 2008. The data set is presented together with the results of a preliminary analysis which are compared to two high frequency ground motion models used for eastern North America ground motion studies.

Digital Data Set

The digital data were obtained from digital waveform archives at Saint Louis University, the CERI at the University of Memphis PANDA experiment and recent recordings of the CERI broadband network. The original waveforms were deconvolved to ground velocity and parametric data were derived from each seismogram. Given the ages of the data set, considerable effort will be required to create a waveform database with appropriate instrument responses for preservation. Figure 2.1 shows the locations of the earthquakes and stations that comprise this data set.

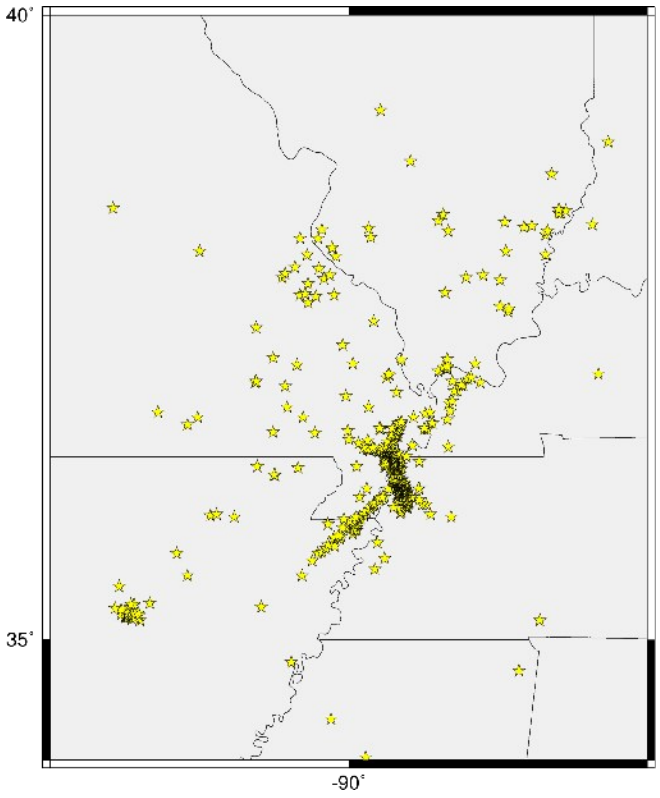

Fig. 2.1(a). Distribution of earthquakes used to form this data set.

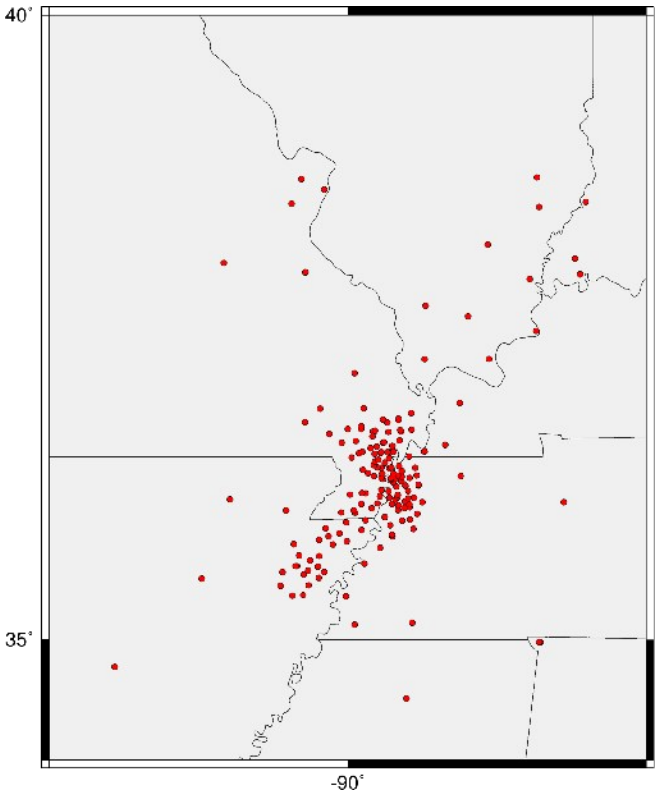

Fig. 2.1(b) Distribution of seismograph stations used for this data set.

The earthquakes were selected to provide a uniform distribution of distance and magnitude. Figure 2.2 highlights this aspect of the data set. The event locations and local magnitudes are taken from the CERI database: (http://www.ceri.memphis.edu/seismic/catalogs/cat_nm.html)

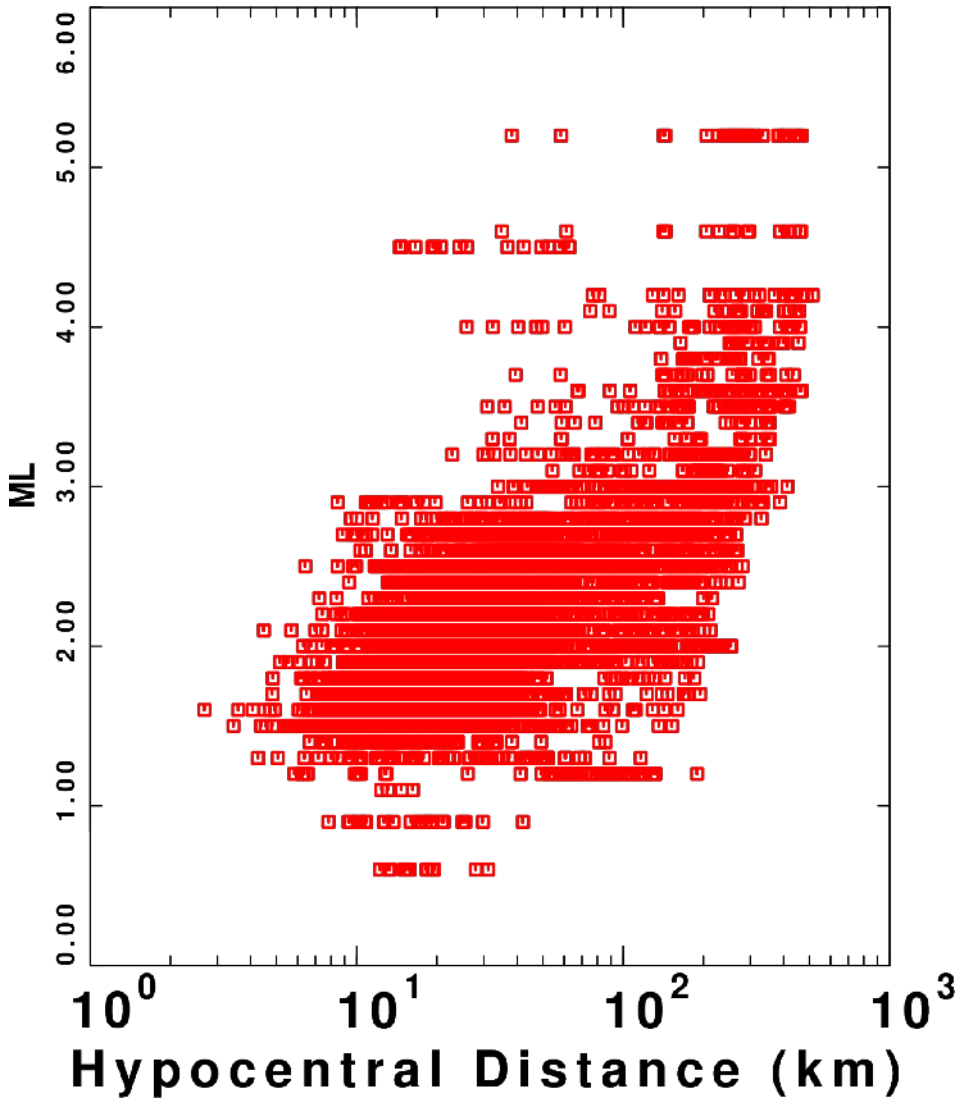

Fig. 2.2. Distribution of waveform data in the data set as a function of hypocentral distance and M_L magnitude.

Because of the distribution of stations and earthquakes, ground motion is well sampled from 10 to 400 km. However, the range of local magnitude, M_L, is not sufficient to investigate ground motions for large earthquakes. No direct relationship has been derived from the M_L and Mw for this study region. The moment magnitudes are taken from the tabulation of moment tensor inversions for North American earthquakes is given at the link

http://eqinfo.eas.slu.edu/Earthquake_Center/MECH.NA/MECHFIG/mech.html .

Of the 632 earthquakes in the data set, 12 correspond to events used in this study (Table 2.1). Figure 2.3 shows the Mw vs catalog magnitude relation for these events.

Table 2.1. Comparison of Moment and Catalog Magnitudes

EVT ID	YEAR	MON	DAY	HR	MIN	M_W	M_L	H (km)	Ref
193	1991	5	4	1	18	4.13	4.5	8	SLU
343	2003	6	6	12	29	4.02	4.0	5	SLU
517	2004	7	16	3	25	3.46	3.5	5	SLU
646	2005	2	10	14	4	4.11	4.1	14	SLU
647	2005	5	1	12	37	4.22	4.2	8	SLU
648	2005	6	2	11	35	3.89	3.6	15	SLU
649	2008	2	20	12	21	3.60	3.6	4	SLU
650	2008	4	18	9	37	5.23	5.2	14	SLU
651	2008	4	18	15	14	4.61	4.6	14	SLU
652	2008	4	21	5	38	4.00	4.0	15	SLU
653	2008	4	25	17	31	3.72	3.7	13	SLU
654	2008	6	5	7	13	3.36	3.4	17	SLU

SLU: http://eqinfo.eas.slu.edu/Earthquake_Center/MECH.NA/MECHFIG/mech.html

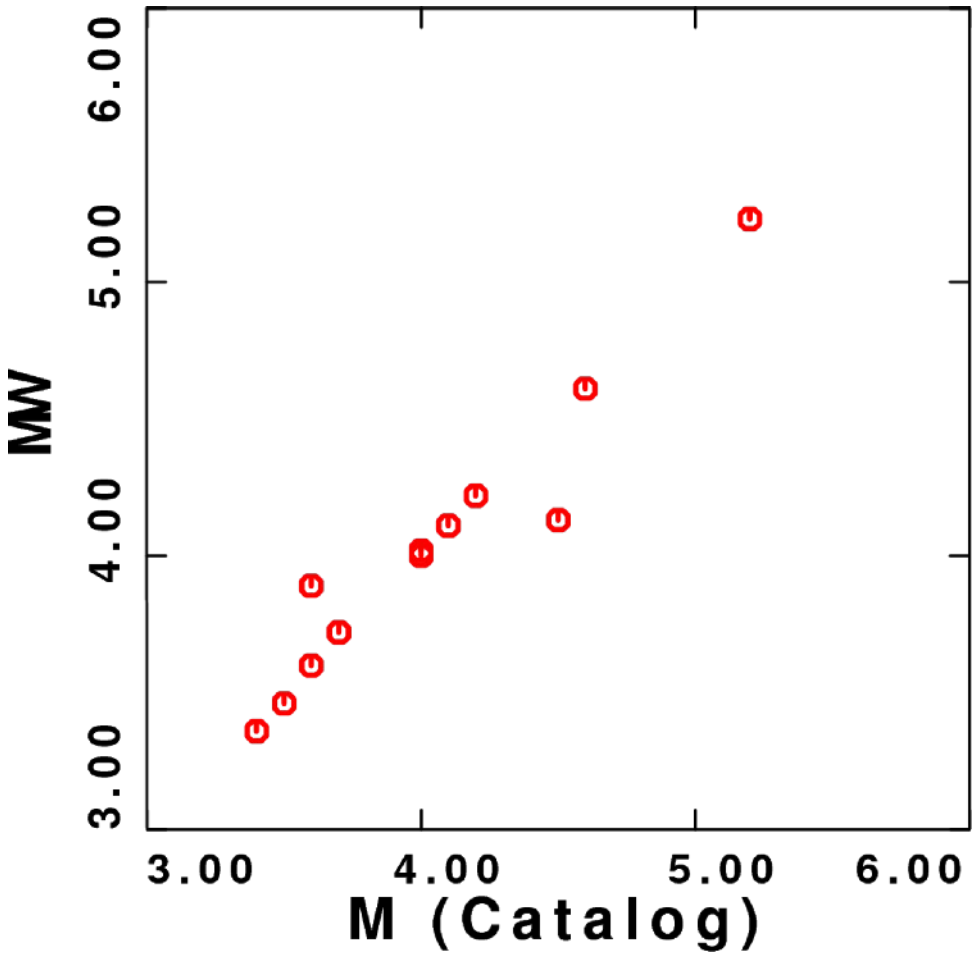

Fig. 2.3. The MW vs catalog magnitude data set. The catalog give one magnitude which may be Lg, duration or even Mw. So the 1-1 fit is not surprising.

Data Processing

The creation of the tabular information for data analysis used three datasets: the Saint Louis University digital data recorded 1980-1992 on a PDP 11/34, the 1990-1991 PANDA data set, and more recent triggered broadband data from CERI at the University of Memphis. The 1980-1992 data set was deconvolved using recursive digital filters and the PANDA and recent data sets using the polezero files with SAC. The sampling rate and corresponding Nyquist frequency were noted. When using SAC a frequency domain deconvolution was used to yield ground velocity in m/s after applying a zero-phase bandpass filter that tapered the ground motion spectrum to zero from 1/2 the Nyquist frequency to the Nyquist frequency. The 1/2 Nyquist frequency was selected since this would ensure at least 4 points per cycle to define a sine/cosine wave.

Next the ground velocity are examined and the P- and S-wave first arrivals are selected. These instrument deconvolved traces are examined for glitches and data gaps.

The last stage is to derive ground motion parameters from each trace. Since the SLU approach (Raoof, 1999; Malagnini et al ,2000a,2000b; Malagnini and Herrmann, 2000) focuses on a complete description of the S-wave ground motion duration, peak motion and spectra are measured. Each

waveform is passed through a sharp bandpass filter. We use filter center frequencies, fc, of 1, 2, 3, 4, 6, 8, 10, 12, 14 and 16 Hz. For each center frequency, the trace is high-pass filtered with an 8-pole Butterworth filter with corner frequency fc/1.414 and then low-pass filtered with an 8-pole Butterworth filter with corner frequency of 1.414 fc. The filtering is not performed unless the center frequency is less than ½ the Nyquist frequency. For each filter frequency, the duration is estimated as the time window between the 5% and 75% limits of the integrated squared velocity of the signal following the S arrival, and the Fourier velocity spectrum is obtained from the RMS spectra within the two bandpass filter corners. In addition, the spectral moments and the duration are used to estimate a predicted peak motion and corresponding confidence limits from Random Vibration Theory. Other trace parameters include the signal envelope for use in later S/N tests.

After trace parameters are determined for all traces for all events, a regression analysis is performed. The first step is to parameterize the separate peak filtered velocity and Fourier velocity data sets. This is done using a model

$$\log A = E + D + S$$

where A is either the peak filtered ground velocity (m/s) or the Fourier velocity spectra (m). D is a distance term which is forced to be 0 at a distance of 40 km. The S is a site term, which is constrained such that the sum of all vertical site terms is zero. The horizontal term is permitted to float. The distance function, D, is a piecewise linear function defined by a finite set of nodes. A differential smoothing operator is applied to the D term to yield a smooth dependence with distance. The excitation term, E, is related to the source and also actual propagation because of the constraint on the D term. For this data set, E is the level of motion at a distance of 40 km. The D term propagates that level to the the particular observation distance, and the S term permits a local site modification. The S constraint forces E to be defined as the expected network-average vertical motion at a distance of 40 km. The reasons for constraining the vertical component is due to the fact that older data sets usually consist of only vertical component data and also because the site effect of local site effects on the vertical component of the ground motion should not be as variable as for the horizontals under the assumption that the vertical motion on soft soil sites is the result of a P-wave incident at the surface because of an S-to-P conversion at the base of the sediments.

The regressions are performed using the separate peak filtered ground velocity and the Fourier velocity spectra data sets at the individual frequencies. The purpose of this extra effort is to ultimately define a parametric model for ground motion prediction based on stochastic or random vibration theory (e.g., Boore, 2000), which requires that the model correctly match the observed Fourier spectra, peak motion and duration. This approach also recognizes the practical problems inherent in the data sets. The time-domain peak motion is the simplest to determine. The determination of the Fourier spectrum requires the specification of a signal window, the same used for the duration measurement; this is not easy to accomplish for noisy signals. However to model the observations, the prediction of peak motion takes much longer than the estimation of the spectra.

Data Quality Check

One way to check the data is to compare the regression results to predictions based on published models.

Regression results and forward modeling

The next table indicates the number of waveforms used in the regression analyses. Before permitting an event to be included in the regression, we required that there be at least 4 waveforms (e.g., at least 2 stations since we have verticals and horizontal recordings) for that event. The number of peak filtered velocity waveforms is greater than this used for the Fourier velocity because of the application of the criteria that the Fourier velocity value together with the estimated duration be compatible with the random vibration theory estimate of the peak value. This was done because the value of the Fourier velocity spectra depends upon the duration window used and the duration is difficult to compute automatically in the presence of noise.

Number of waveforms for regression at each center frequency

Center Frequency (Hz)	Fourier Velocity	Peak Velocity
1	631	2085
2	2246	5227
3	3569	7953
4	4587	9804
6	6167	11960
8	6852	12598
10	6674	12741
12	5858	12549
14	4864	11988
16	4283	11370

Because of the need to always question instrument calibration, we apply a coda normalization technique to provide an independent estimate of the spectral amplitude versus distance relation. The coda normalization (Aki, 1980; Frankel at al, 1990) aligns the coda of all events and then plots the rescaled peak motion or Fourier velocity spectra as a function of distance. This procedure thus corrects for the source input at the given frequency and also for incorrect instrument response. It is limited by not having a time series long enough to define the coda level, especially at large distances, which is often the case with triggered data.

The peak motion or Fourier velocity spectra are then processed according to the regression equation defined above. Figure 2.4 compares the two independent estimates of the amplitude versus distance estimate at frequencies of 2 and 16 Hz. The comparison is good at high frequency but fails for low frequencies. We have noted this before for the New Madrid data set but not for data sets in other regions. Perhaps the failure of the comparison at the low frequency is due to the need for a coda shape factor that depends upon epicentral distance (Mayeda et al., 2003) or the assumption that the coda shape is identical for both vertical and horizontal components. The regression residual plot emphasizes that the distance range of 10 – 400 km is well sampled. There are 2246 and 4283 observations in the 2 and 16 Hz Fourier velocity data sets, respectively. In addition, the residual plot shows no obvious

distance trends.

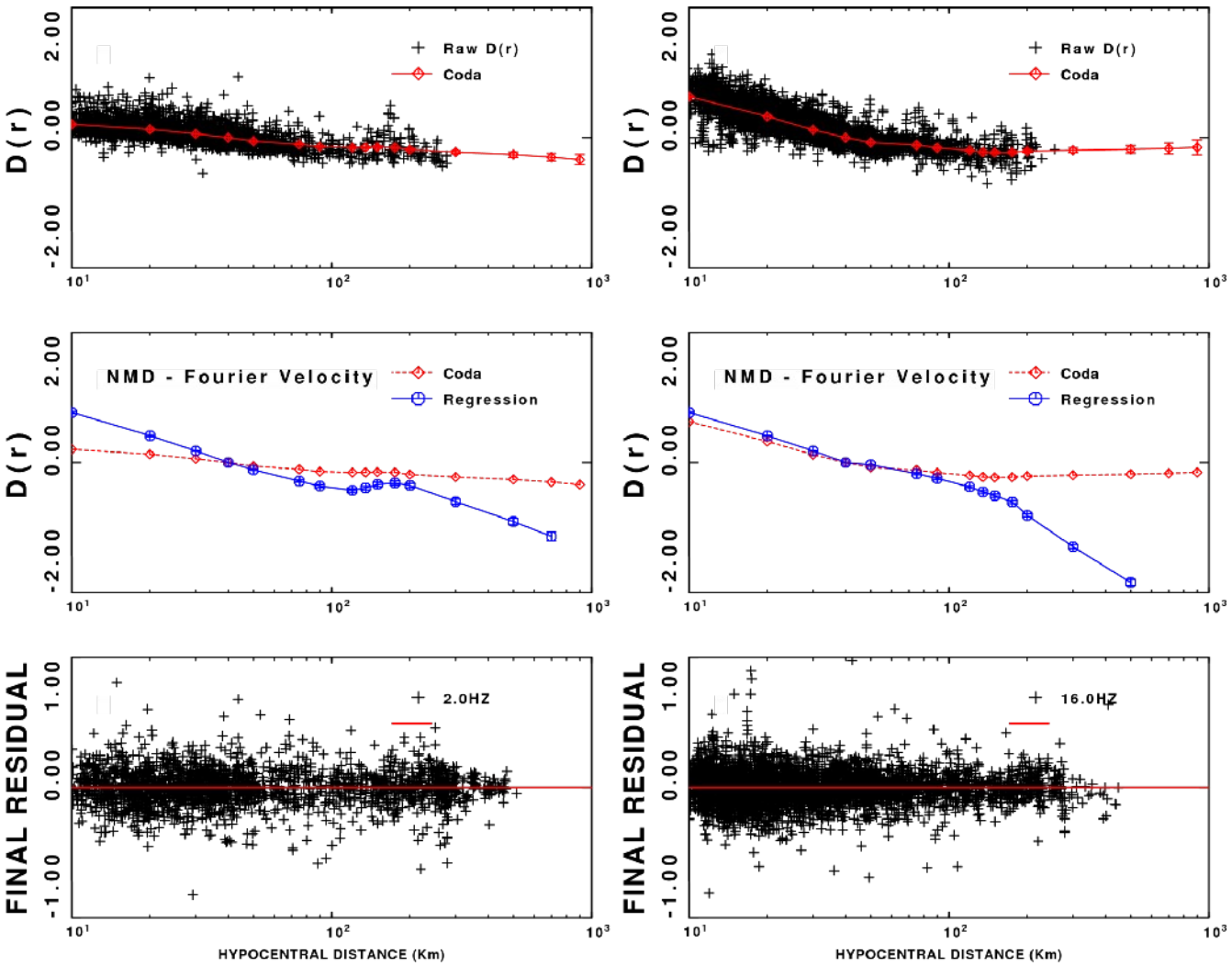

Fig. 2.4. Data set comparison for 2 Hz (left) and 16 Hz (right). Top - coda scaled amplitudes as a function of distance with a regression curve (red); Center – comparison of coda estimate (red) to the regression results (blue); Bottom – residuals from the regression analysis as a function of distance.

Forward modeling consists of defining the ground motion as a function of moment magnitude and distance. To accomplish this, we started with the SMSIM package of Boore (2002), replaced proprietary *Numerical Recipes* subroutines with open-source equivalents, and then constructed a new external wrapper so that the programs can be run using a simple control file and command line arguments. The programs are called *fscal* to predict the Fourier spectra, *tdcal* to predict peak motion in the time domain through a stochastic, filtered white noise simulation, *rvcal* to predict peak motion using random vibration theory, and *tscal* to create a simulated time series. The internal routines that compute peak motions or spectra are those of Boore (2000).

We compare the D(r) term and the E(f, 40 km) terms to predictions based on two separate models: Atkinson and Boore (1995) and Atkinson (2004), since these are the *de facto* standards for comparison.

The control files used are tabulated in the Appendix of this report. Rather than plotting our D(r) term, we plot the frequency dependent residual. We present the E(f, 40 km) for events with known moment magnitude.

Fourier Velocity Data Set

Figures 2.5 and 2.6 compare show the D(r) residuals for the Atkinson and Boore (1995), AB85, and Atkinson (2004), A2004. models, respectively. The fact that the 1 Hz values are not in agreement at short distances is a problem of signal to noise as well as a problem of isolating the S-wave arrival from the P-wave at short distances, especially at low frequencies.

At short distances, e.g., 10 km, the AB95 model slightly under-predicts motions while the A2004 model over-predicts. In the 40-150 km distance range, both models under-predict the motion at higher frequencies.

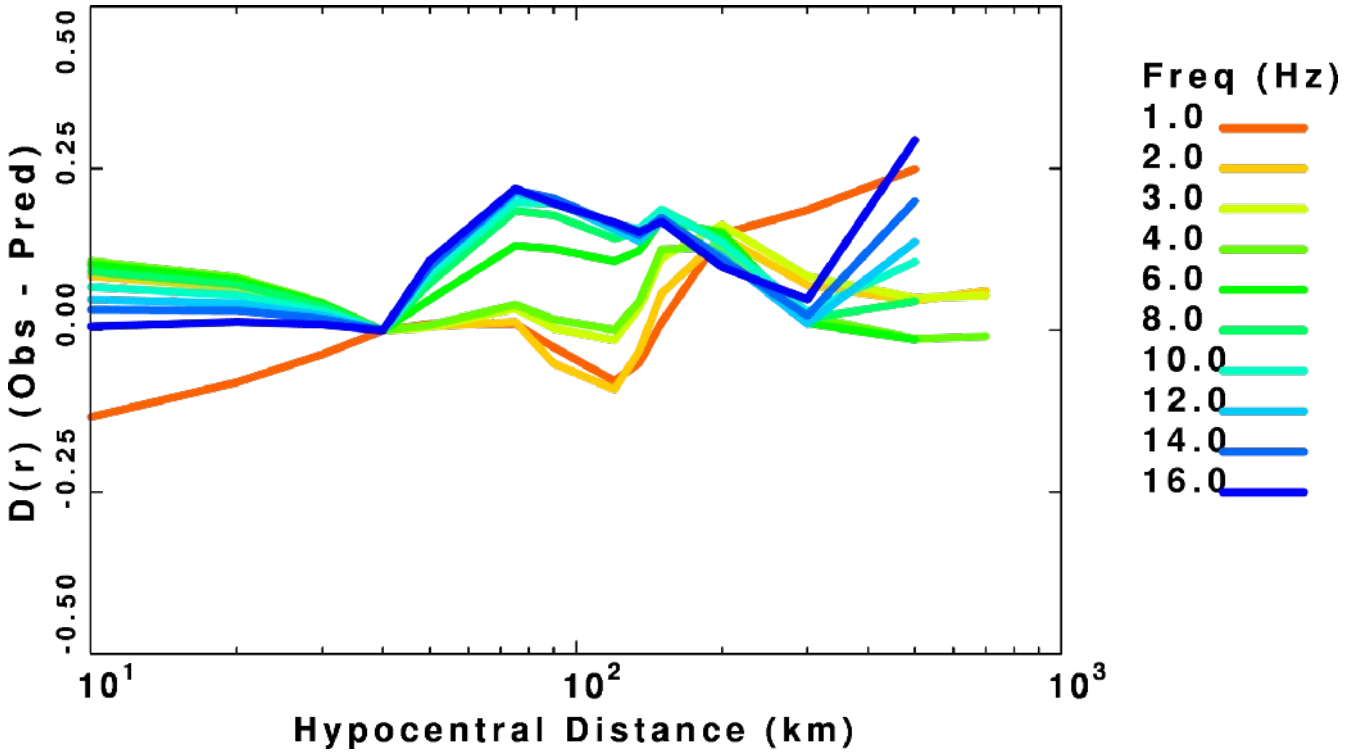

Fig. 2.5. Difference between regression D(r) and the predictions based on the Atkinson and Boore (1995) model.

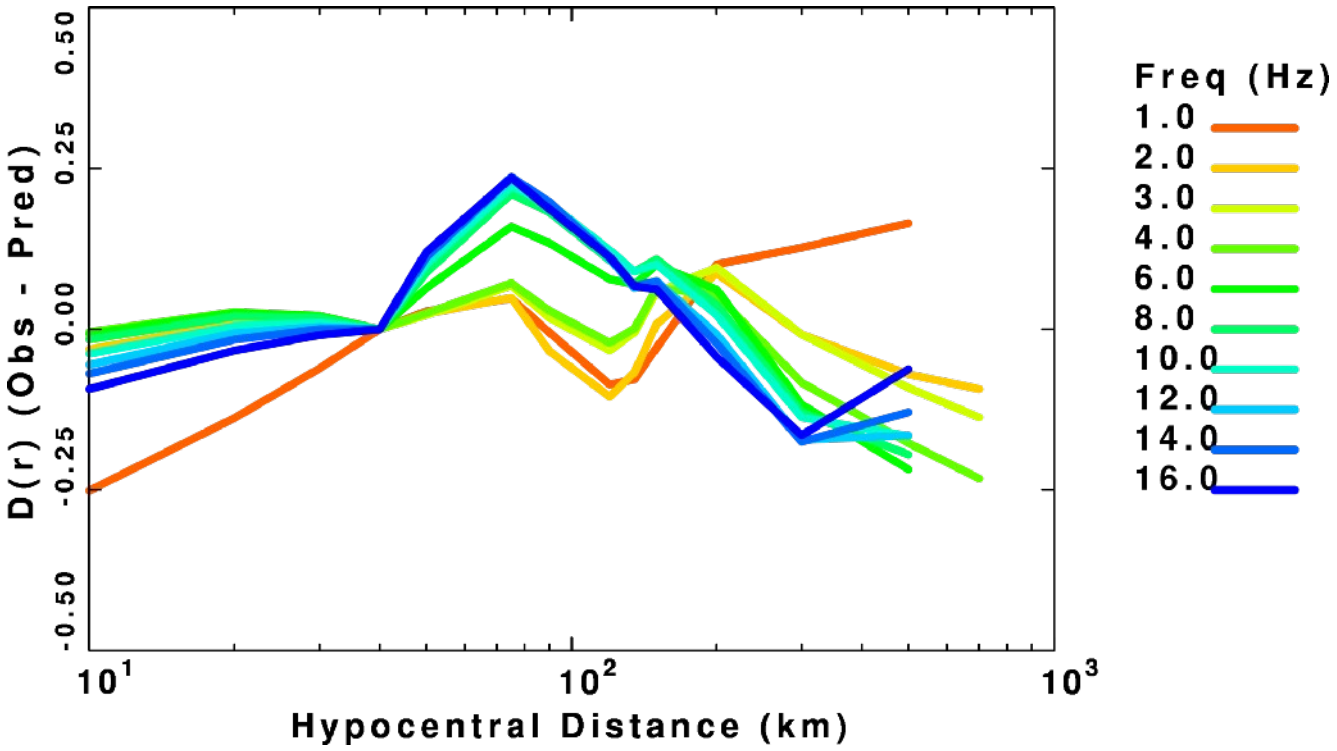

Fig. 2.6. Difference between regression D(r) and the predictions based on the Atkinson (2004) model.

Figures 2.7 and 2.8 compare the predicted and regression E(f, r=40 km) values. To obtain the predicted values, the source spectrum is defined for a given moment magnitude, which is then propagated out to a distance of 40 km, accounting for geometrical spreading and anelastic attenuation of the models. The effect of 'kappa' and/or f_{max} is included at this point. The observed excitations are plotted for the events with know moment magnitude.

We now focus on the predictions of the two models formulated in Appendix A.

Figures 2.7 and 2.8 compare the observed and predicted excitations for the Atkinson and Boore (1995) and Atkinson (2004) models. It is difficult to distinguish the differences between the model since the predicted excitation at 40 km depends not only upon the source scaling but also on the geometrical spreading and also on the effect of the Q(f) term which is different for the two models.

To hightlight the differences in the predictions, Figure 2.9 presents the differences between observed and model predicted excitations for the two models for events with known moment magnitude. The positive residuals associated with the Atkinson (2004) model at the lower frequencies indicates that the model under-predicts the observed level of vertical component excitation. On the other hand, both model predictions seem equally compact indicating that the spectral scaling cannot be distinguished for earthquakes of the size considered here.

Because we permitted the horizontal component site term to be unconstrained, we are able to compute an H/Z ratio. Figure 2.10 compares the H/Z ratio, with two ratios per station. For comparison Equation (8) of Atkinson (2004) is plotted.

In spite of these differences, this exercise indicates that the data set is adequate for regression analysis as part of the NGA-EAST process once the data are QC checked again.

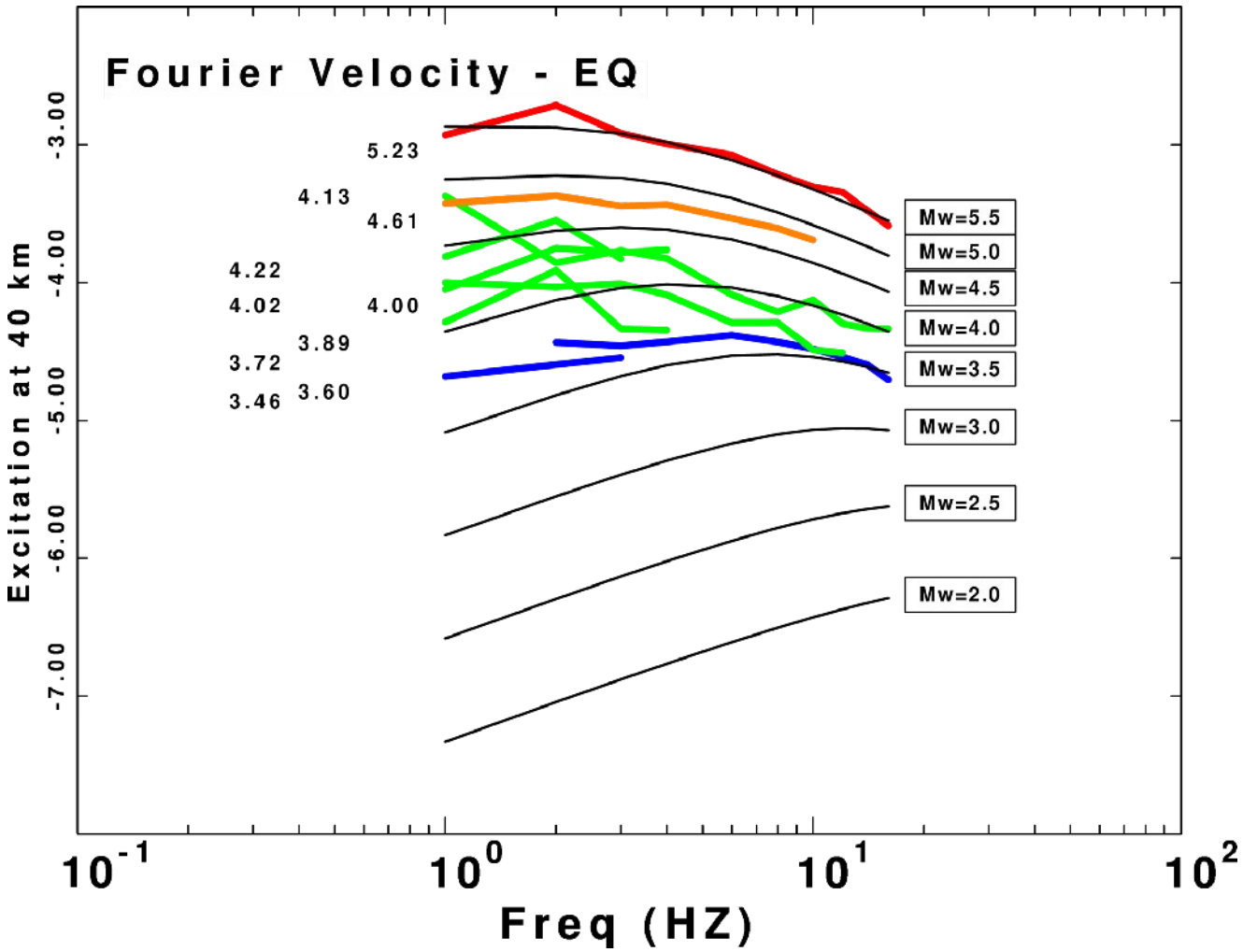

Fig. 2.7. Comparison of predicted (black) and regression determined Fourier velocity excitation (color) terms at 40 km for the Atkinson and Boore (1995) model. The predictions are annotated with the moment magnitude at the right. The moment magnitudes for the observed data at plotted at the corresponding 1 Hz levels on the left.

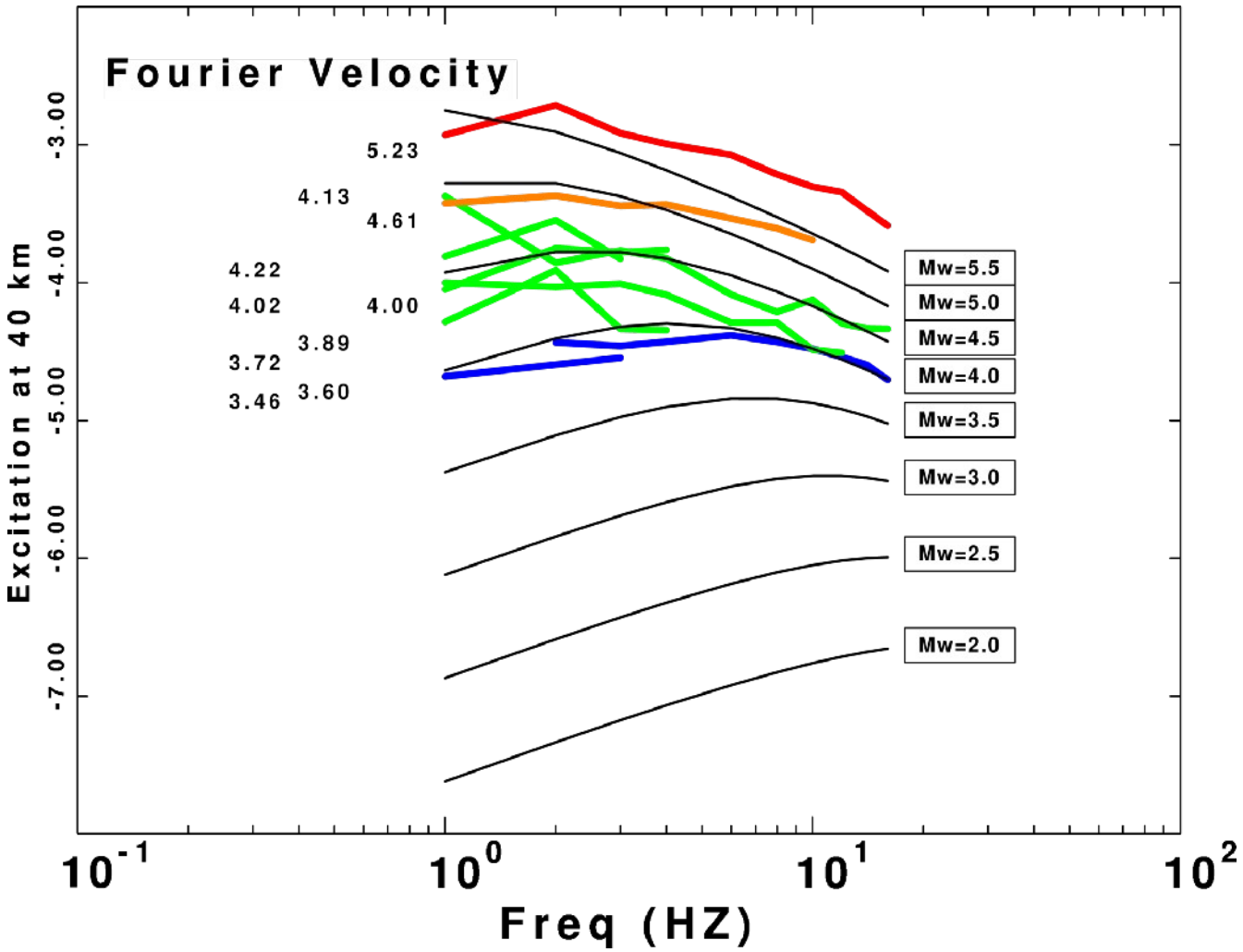

Fig. 2.8. Comparison of predicted (black) and regression determined Fourier velocity excitation (color) terms at 40 km for the Atkinson (2004) model. The predictions are annotated with the moment magnitude at the right. The moment magnitudes for the observed data at plotted at the corresponding 1 Hz levels on the left.

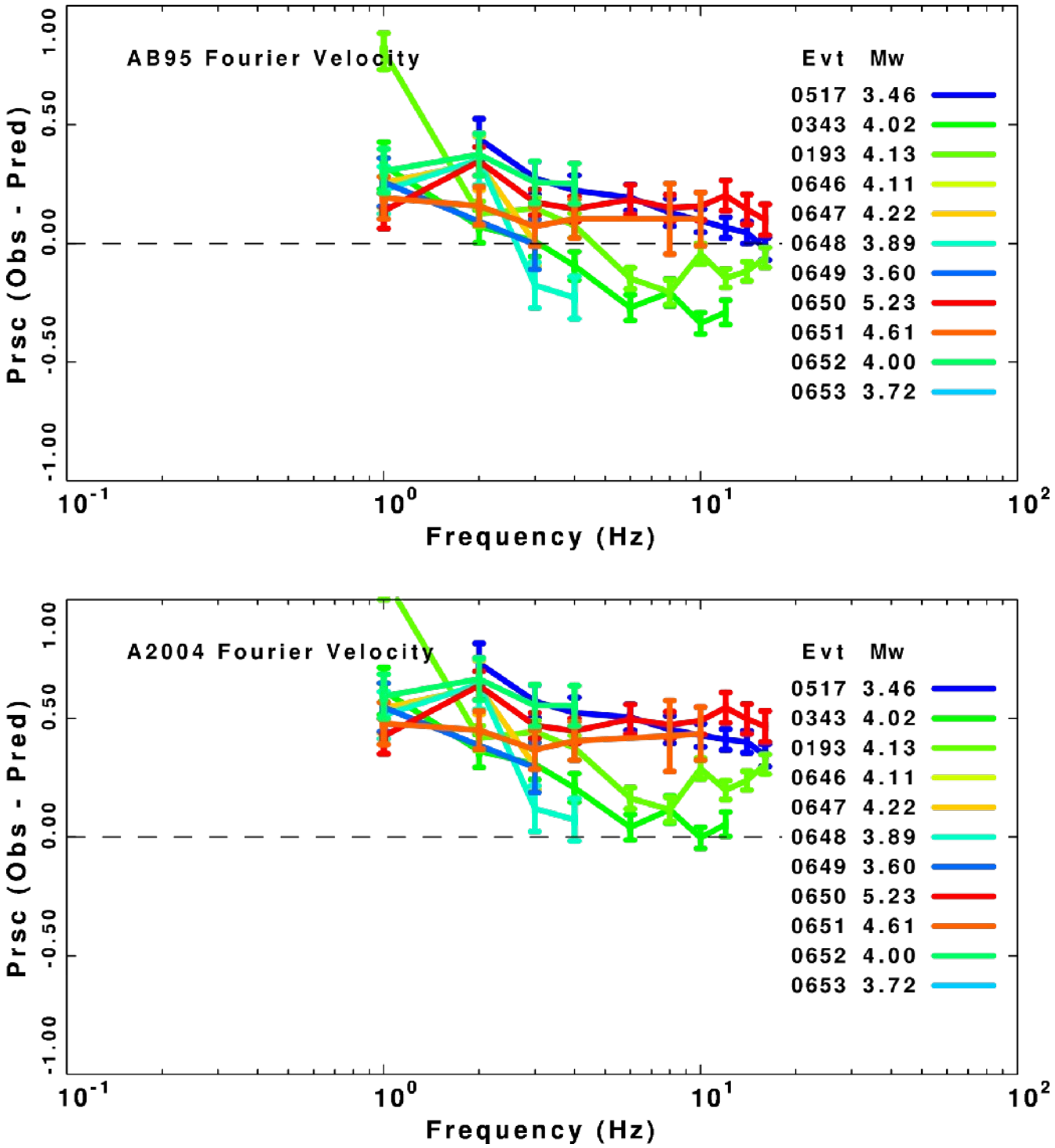

Fig. 2.9. Difference between the observed and predicted excitations for Fourier velocity at 40 km. The predictions are based on the Atkinson (2004) model with a 200 bar stress drop. The colors are keyed to the event number and the moment magnitude.

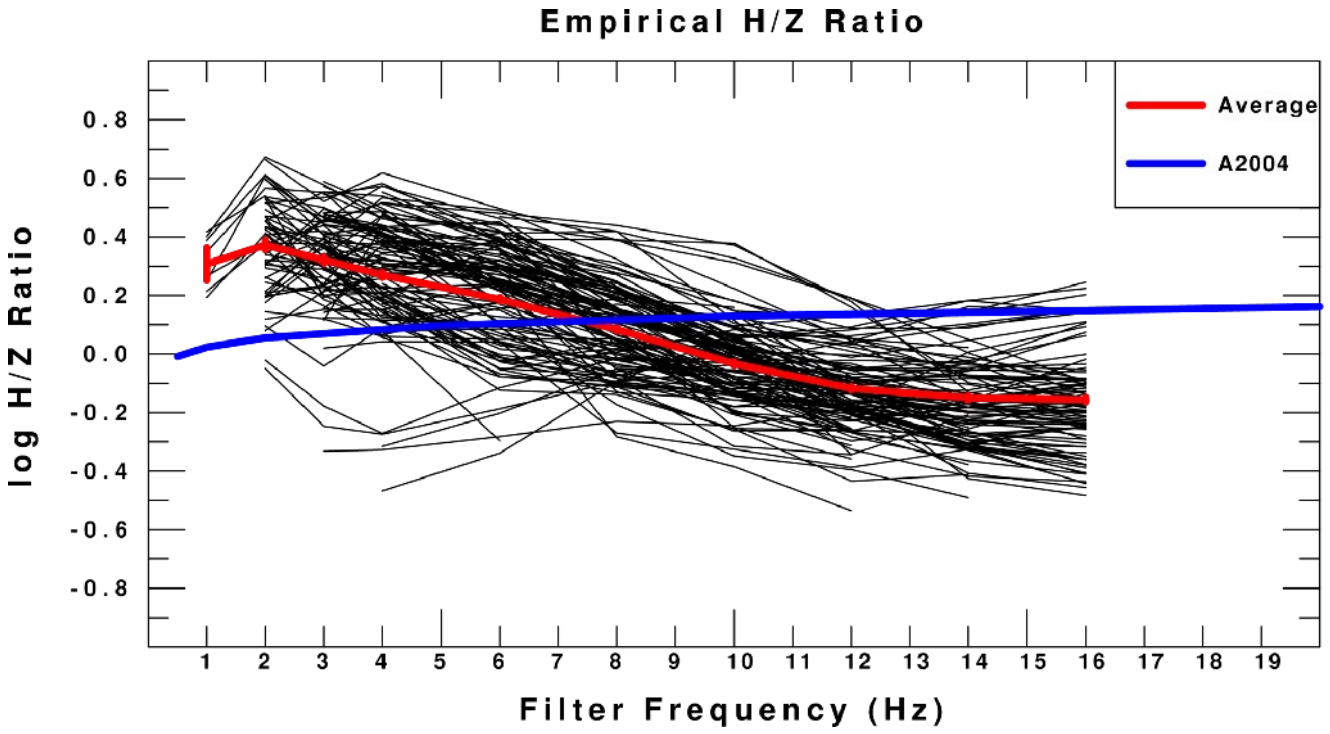

Fig. 2.10. Individual H/Z estimates (black curves) from the three-component data set of Fourier velocity. The red curve is the mean of all black curves. For reference Equation (8) of Atkinson (2004) is plotted.

Peak Filtered Velocity Data Set

We next present the regression results using the peak filtered time-domain amplitudes. As mentioned earlier, the observed peak values are direct measurements and do not require the specification of the signal window required for the Fourier velocity spectra estimate. However, the forward prediction from the model requires a specification of the spectra and the duration. These data represent those values which have a signal-to-noise ratio ≥ 4.

Figure 2.11 compares the regression D(r) results for center frequencies of 2 and 16 Hz to the estimates using the coda normalization technique. We again see problems in the implementation of the coda normalization technique at low frequencies. At 16 Hz the two estimates of D(r) are quite similar, indicating that combining two instrumental data sets for the same region did not introduce any significant biases. We also see that the 2 Hz data seems sufficient out to 400 km while the 16 Hz data may be adequate out to 350 km.

Figures 2.12 and 2.13 present the difference between the D(r) from the regression and each model, Figures 2.14 and 2.15 present a comparison of the E(f, r=40 km) and Figure 16 presents the difference between the observed and predicted excitations.

The D(r) residuals again show that the AB95 model fits better than the A2004 model at short distances.

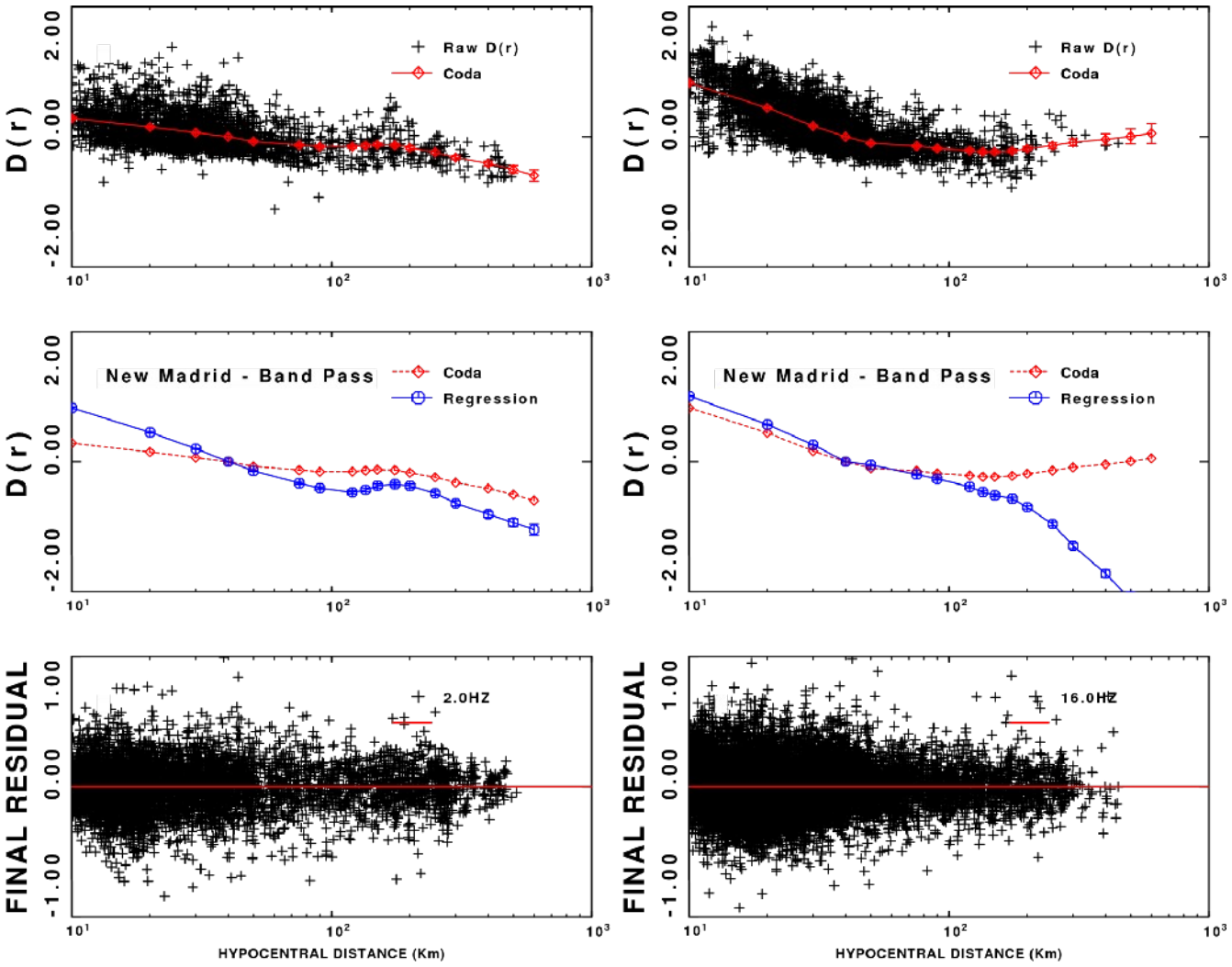

Fig. 2.11. Data set comparison for 2 Hz (left) and 16 Hz (right). Top - coda scaled amplitudes as a function of distance with a regression curve (red); Center – comparison of coda estimate (red) to the regression results (blue); Bottom – residuals from the regression analysis as a function of distance.

At greater distances, the observed motions are greater than the predicted motions, indicating a need to modify both the geometrical spreading term and Q(f) using in the two models.

The comparison of the Excitation terms in Figures 2.14 and 2.15 and the residuals in Figure 2.16 again indicate an under-prediction at lower frequencies of observed vertical component excitation at 40 km by the A2004 model. The AB95 model scaling seems better than the fixed 200 bar stress drop scaling assumed for the A2004 model in that the spread in residuals at any one frequency is smaller. The frequency dependent trends in the residuals of Figure 2.15 indicate the need to use a different Q(f) for this region.

Figure 2.17 presents the H/Z ratio resulting from the regression and compares these to Equation (8) of Atkinson (2004). The error bars on our ratios are not presented. The observed H/Z ratio must be a

characteristic of the deep sediment sites where most of the current three-component stations are located. Thus the observed H/Z ratio as a function of frequency includes the effect of the frequency dependent site amplification and differences in kappa for the vertical and horizontal components.

Finally Figures 2.18 and 2.19 present the duration measurements from from the traces used in the time-domain peak motion data set. There is a significant difference in the duration as a function of frequency, which is related to whether the peak motion is dominated by a single ray at or by a group of ray arrivals.

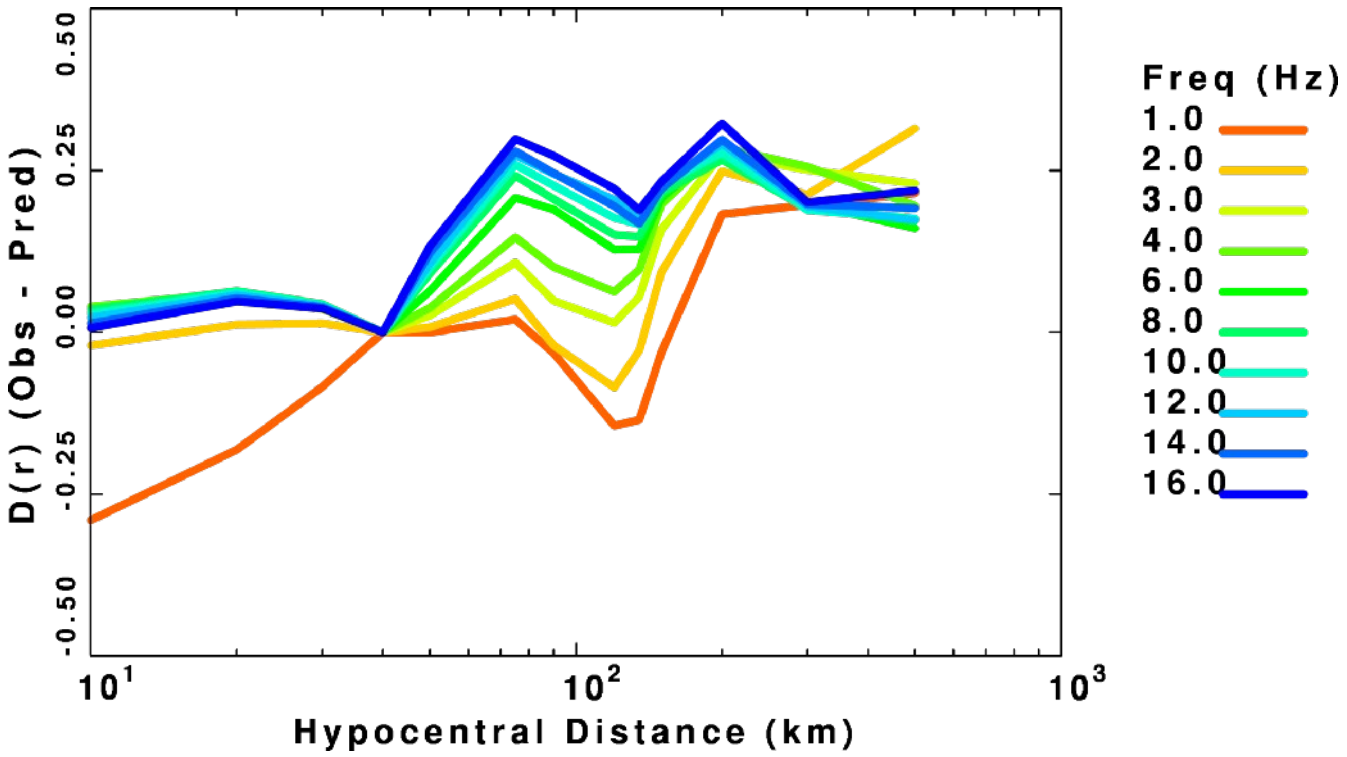

Fig. 2.12. Difference between the time-domain peak filtered velocity regression D(r) and the predictions based on the Atkinson and Boore (1995) model.

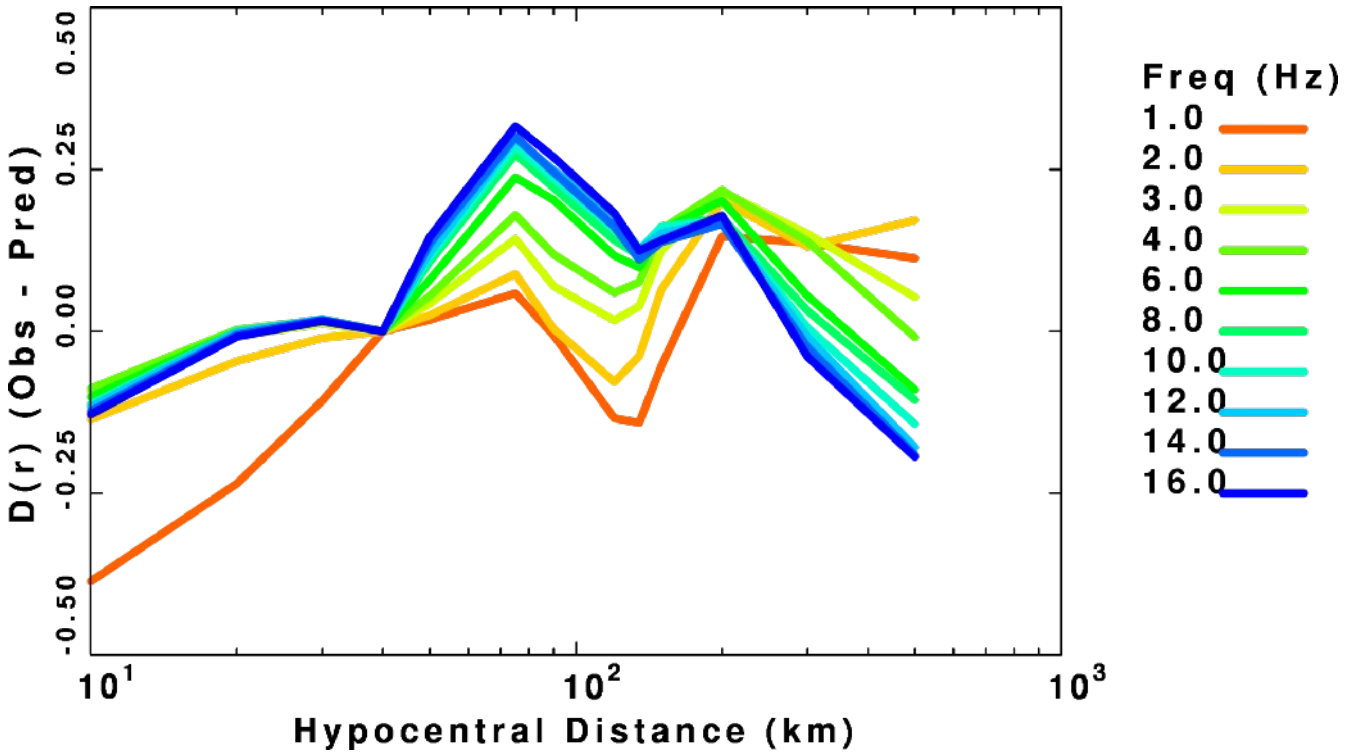

Fig. 2.13. Difference between the peak filtered velocity regression D(r) and the predictions based on the Atkinson (2004) model.

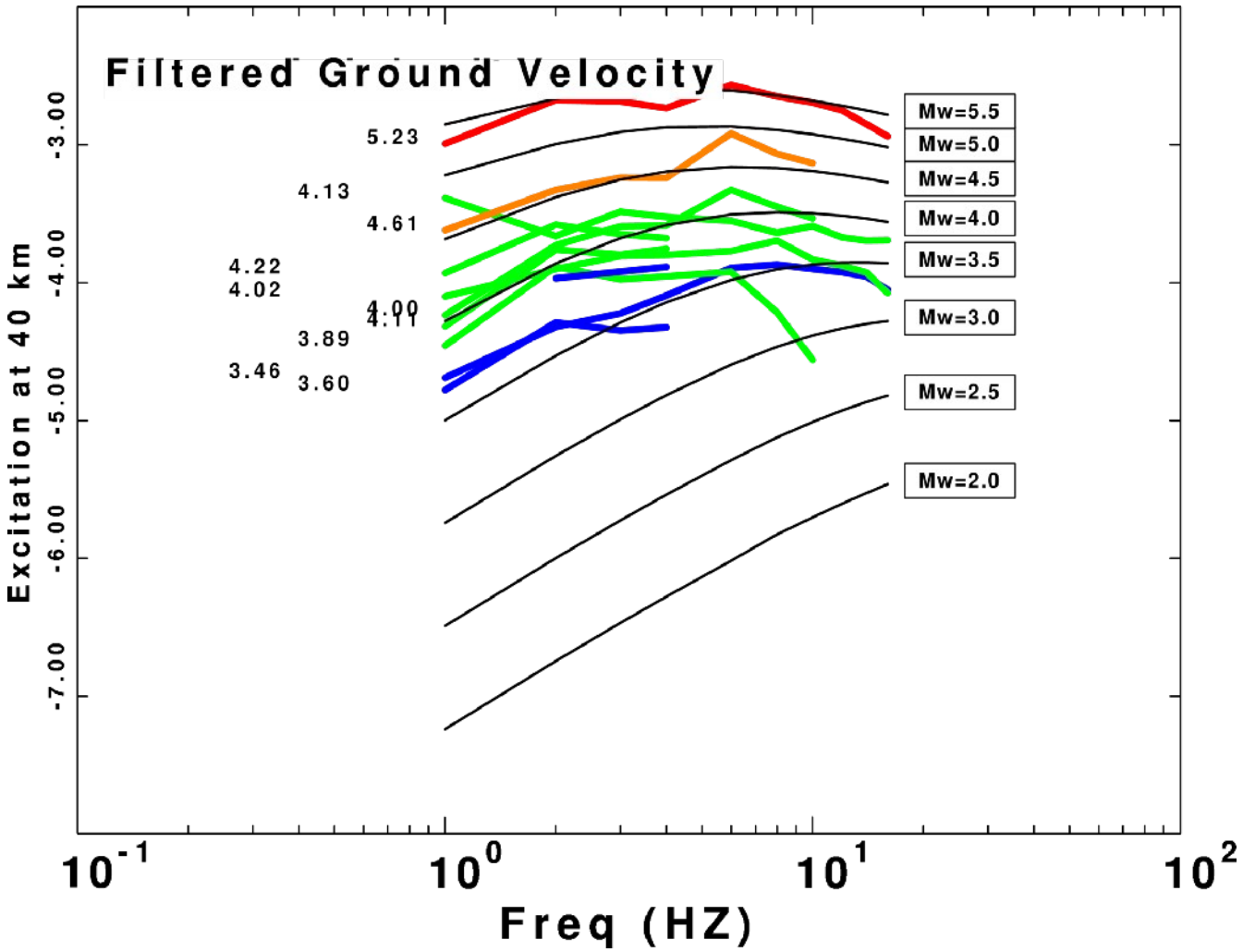

Fig. 2.14. Comparison of predicted (black) and regression determined Fourier velocity excitation (color) terms at 40 km for the Atkinson and Boore (1995) model. The predictions are annotated with the moment magnitude at the right. The moment magnitudes for the observed data at plotted at the corresponding 1 Hz levels on the left.

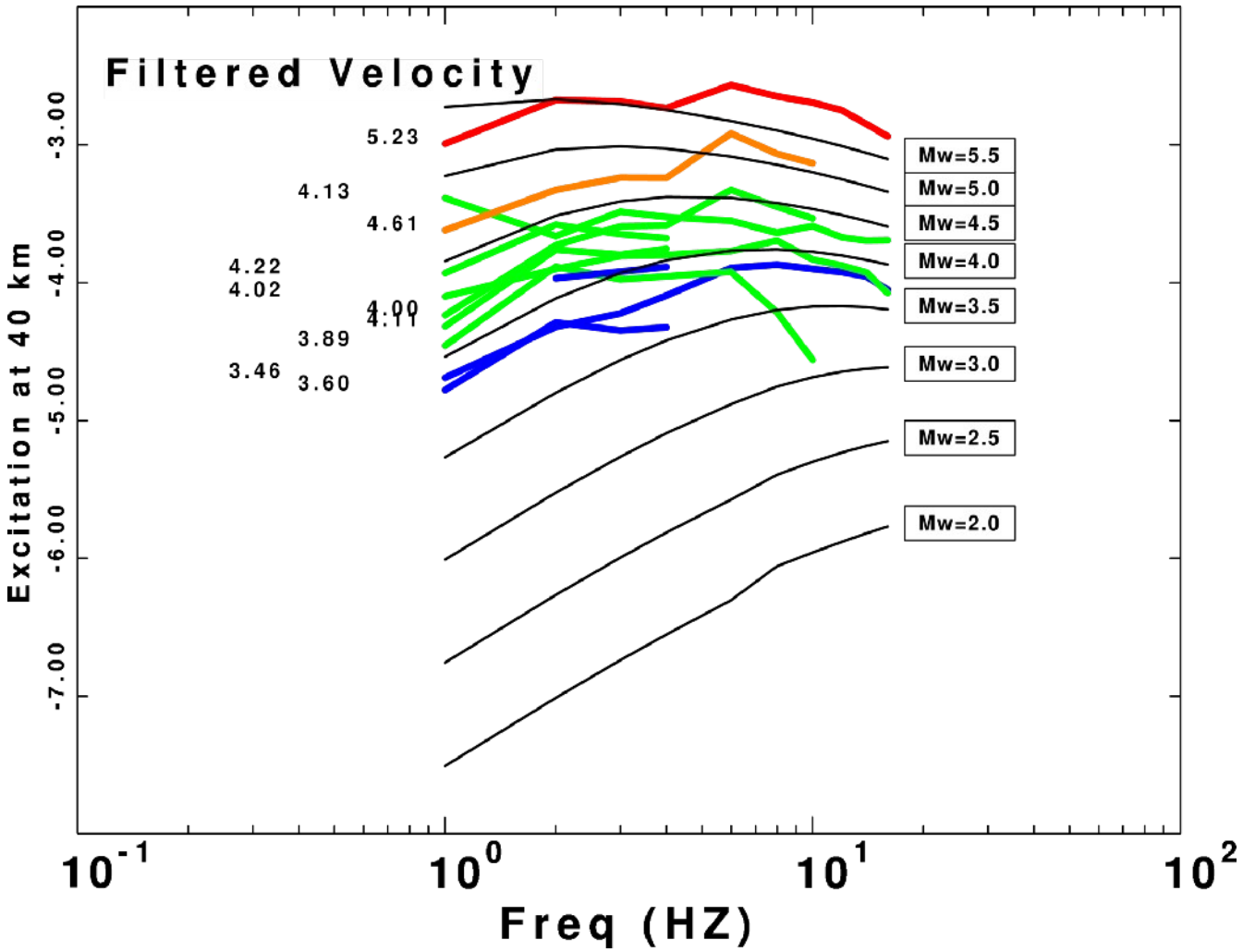

Fig. 2.15. Comparison of predicted (black) and regression determined peak filtered velocity excitation (color) terms at 40 km for the Atkinson (2004) model. The predictions are annotated with the moment magnitude at the right. The moment magnitudes for the observed data at plotted at the corresponding 1 Hz levels on the left.

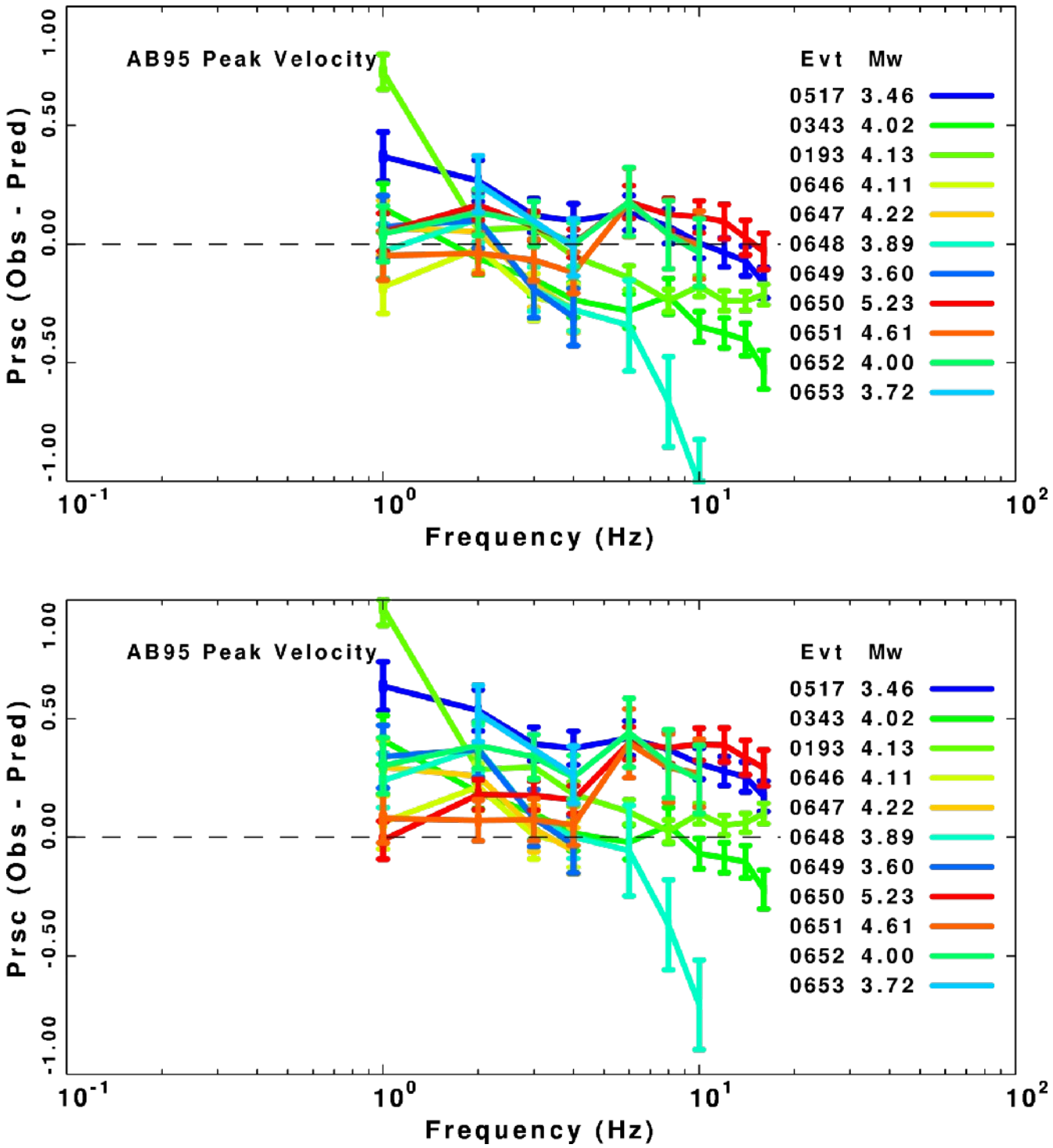

Fig. 2.16. Difference between the observed and predicted excitations for peak filtered velocity at 40 km. The predictions are based on the Atkinson (2004) model with a 200 bar stress drop. The colors are keyed to the event number and the moment magnitude.

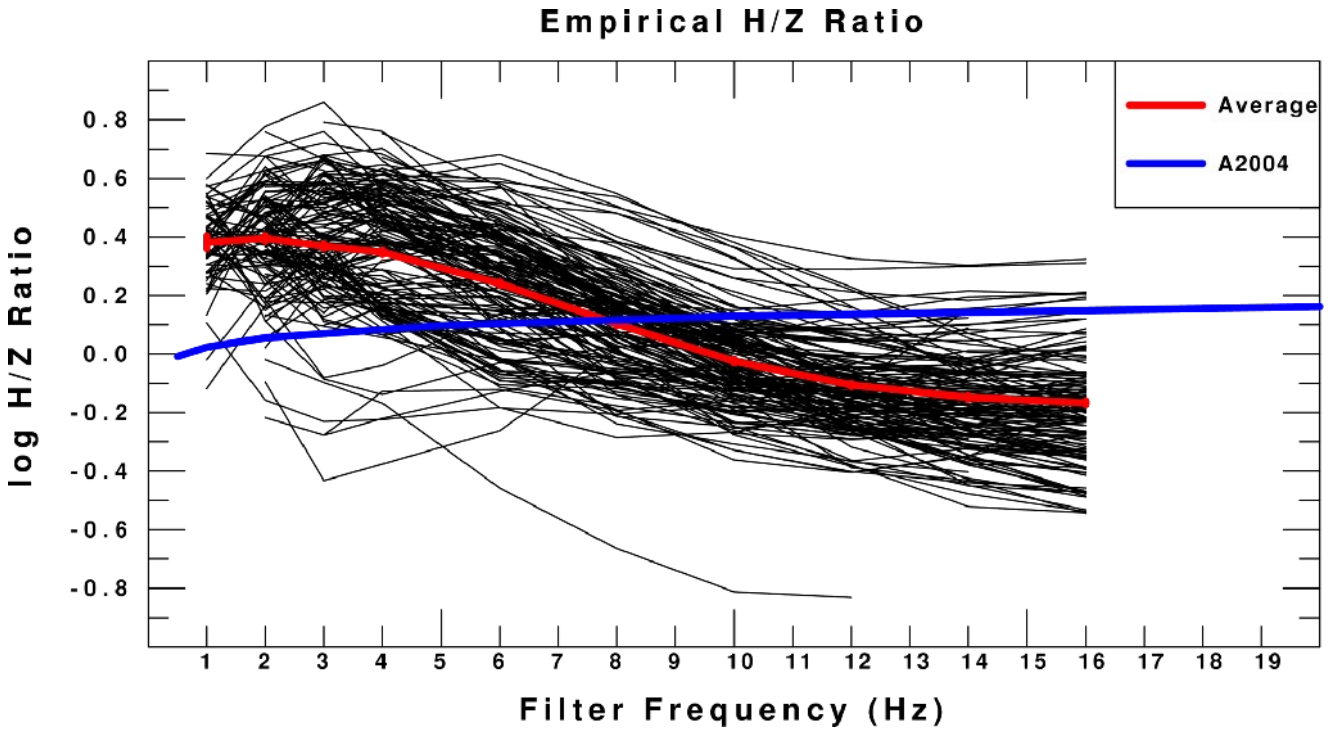

Fig. 2.17. Individual H/Z estimates (black curves) from the three-component data set of peak filtered velocity. The red curve is the mean of all black curves. For reference Equation (8) of Atkinson (2004) is plotted.

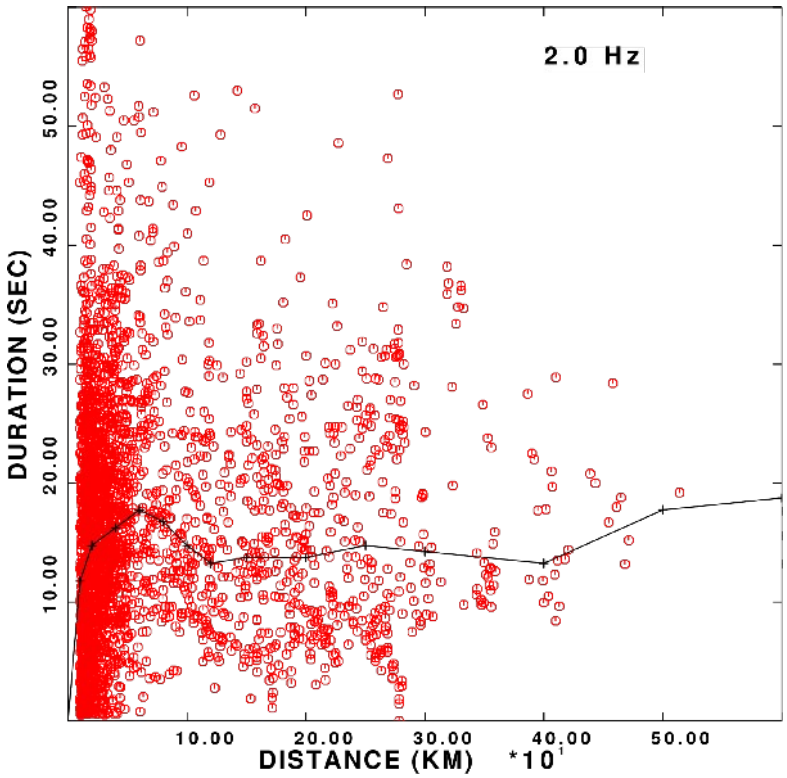

Fig. 2.18. Duration values for the 2 Hz peak velocity data set. The L-1 norm data fit is indicated by the black curve.

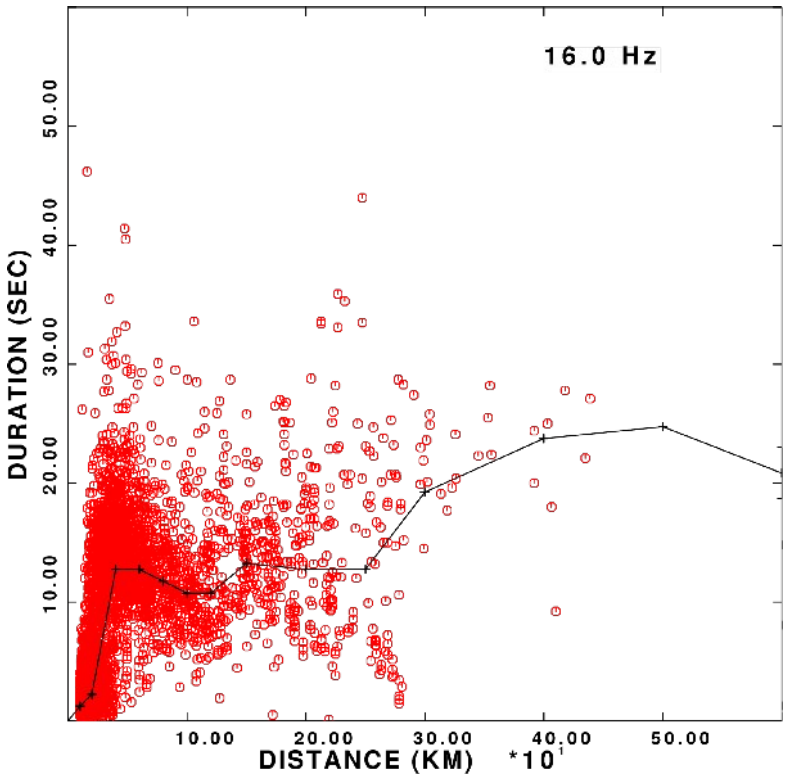

Fig. 2.19. Duration values for the 16 Hz peak velocity data set. The L-1 norm data fit is indicated by the black curve.

3. High Frequency Ground motion data set for Southeast Canada

Revision history:

December 13, 2008:
Event 399 was reexamined. Original waveforms were downloaded from the Geological Survey of Canada autodrm and reprocessed. The previous high frequency with this event was the result of using existing low pass filtered waveforms rather then the original waveforms. This event now can be used for source/propagation scaling tests.

The text now contains plots of the differences between the observed and predicted excitations base on the Atkinson and Boore (1995) and Atkiinson (2004) models.

The text also contains plots of the observed H/Z ratios which are compared to Equation (8) in Atkinson (2004).

June 24, 2010: Added the Mw=5.04 Quebec event of June 23, 2010. The AB95 scaling fits better than my reading of the A2004 scaling. This is the larges event in my data set. I also note in Figures 3.7, 3.8, 3.14 and 3.15 that there is a degree of scatter between observed levels of motion of a nominal Mw=5 event. The detail of the moment tensor inversion is given at the URL

http://www.eas.slu.edu/Earthquake_Center/MECH.NA/20100623174142/index.html

Introduction

This document describes a data set derived from digital recordings of earthquakes in southeastern Canada. The data set consists of 378 earthquakes from September 21, 1993 to November 15, 2008. The data set is presented together with the results of a preliminary analysis which are compared to two high frequency ground motion models used for eastern North America ground motion studies. Several notes are inserted into the text which serve to highlight data set problems or implications that could be address as part of the NGA-EAST process.

Digital Data Set

The digital data were obtained using the AutoDRM of the Canadian National Data Center: http://earthquakescanada.nrcan.gc.ca/stnsdata/autodrm/autodrm_req_e.php. The waveforms were downloaded in a SEED format, which includes the station and component metadata, instrument responses as well as the digital traces. The data set can easily be reconstructed by downloading the files from the data center. Figure 1 shows the locations of the earthquakes and stations that comprise this data set.

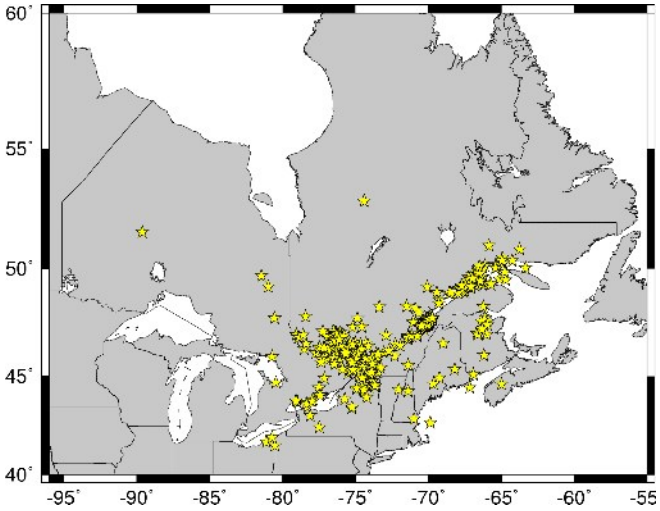

Fig. 3.1(a). Distribution of earthquakes used to form this data set.

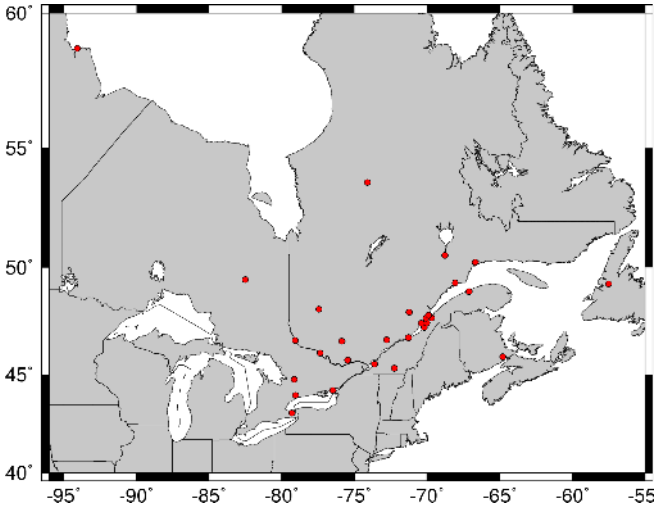

Fig. 3,1(b) Distribution of Canadian digital seismograph stations used for this data set.

The earthquakes were selected to provide a uniform distribution of distance and magnitude. Figure 3.2 highlights this aspect of the data set. The event locations and local magnitudes are taken from the National Earthquake Database of Canada database:

(http://earthquakescanada.nrcan.gc.ca/stnsdata/nedb/index_e.php)

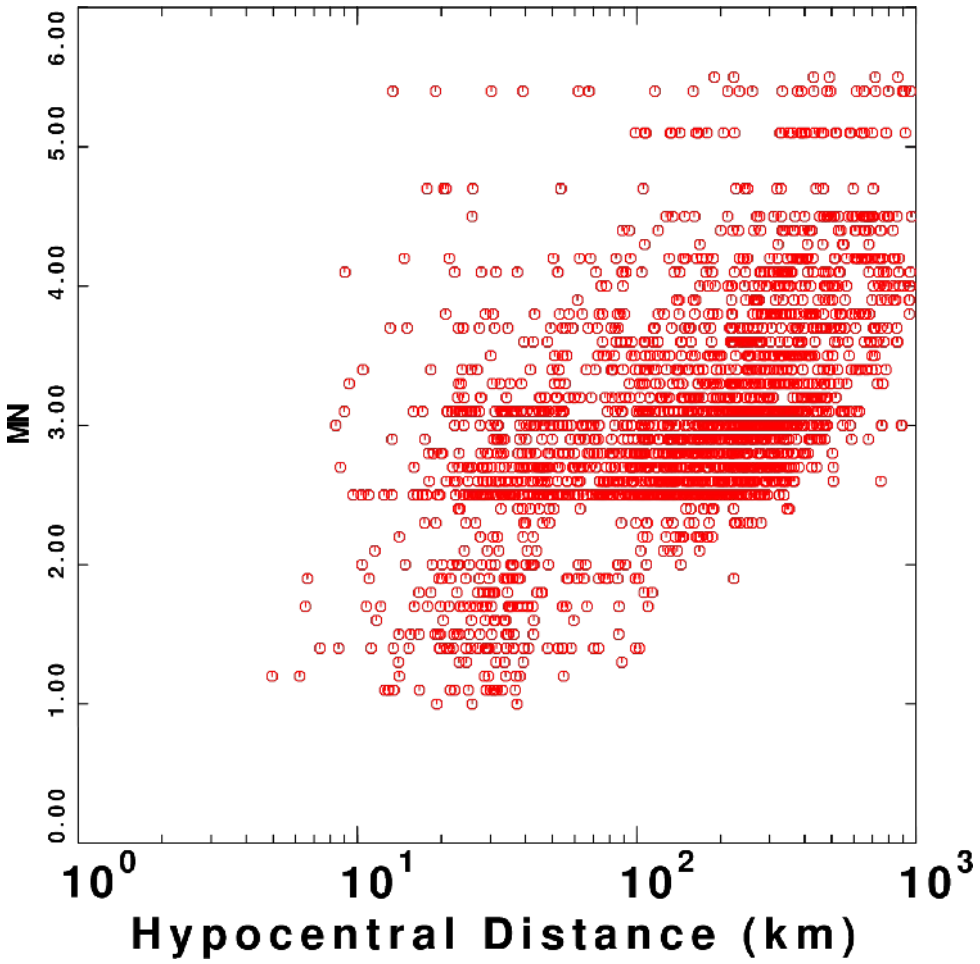

Fig. 3.2. Distribution of waveform data in the data set as a function of hypocentral distance and M_N magnitude.

Because of the distribution of stations and earthquakes, ground motion is well sampled from 10 to 1000 km. However, the range of local magnitude, M_N, is not sufficient to investigate ground motions for large earthquakes. Atkinson (2004) and Atkinson and Boore (1995) discuss the relationship between the bulletin magnitude and moment magnitude M_W. The moment magnitudes are taken from the tabulation of moment tensor inversions for North American earthquakes is given at the link

http://eqinfo.eas.slu.edu/Earthquake_Center/MECH.NA/MECHFIG/mech.html .

Of the 292 earthquakes in the North American data set, 10 correspond to events used in this study (Table 1). These data leads to a regression relation between the two magnitudes:

$$M_W = -0.47\ (\pm 0.45) + 0.95\ (\pm 0.09\ )\ M_N$$

This relation as well as the data in Table 1 are plotted in Figure 3.3.

Table 3.1. Comparison of Moment and Catalog Magnitudes

EVT ID	YEAR	MON	DAY	HR	MIN	M_W	M_N	H (km)	Ref
202	1997	11	06	02	34	4.50	5.1	22	DU
019	1998	09	25	19	52	4.47	5.4	2.5	SLU
337	2002	04	20	10	50	4.97	5.5	10	SLU
338	2002	06	05	20	17	3.64	4.1	9	SLU
273	2003	06	13	11	34	3.34	4.1	9	SLU
001	2005	03	06	06	17	4.58	5.4	12	SLU
397	2005	10	20	21	16	3.61	4.3	10	SLU
398	2006	02	25	01	39	3.62	4.5	16	SLU
399	2006	04	07	08	31	3.77	4.1	25	SLU
396	2008	11	15	10	52	3.57	4.2	14	SLU
400	2010	06	23	17	41	5.04	5.7	22	slu

SLU: http://eqinfo.eas.slu.edu/Earthquake_Center/MECH.NA/MECHFIG/mech.html
DU: Du et al., 2004.

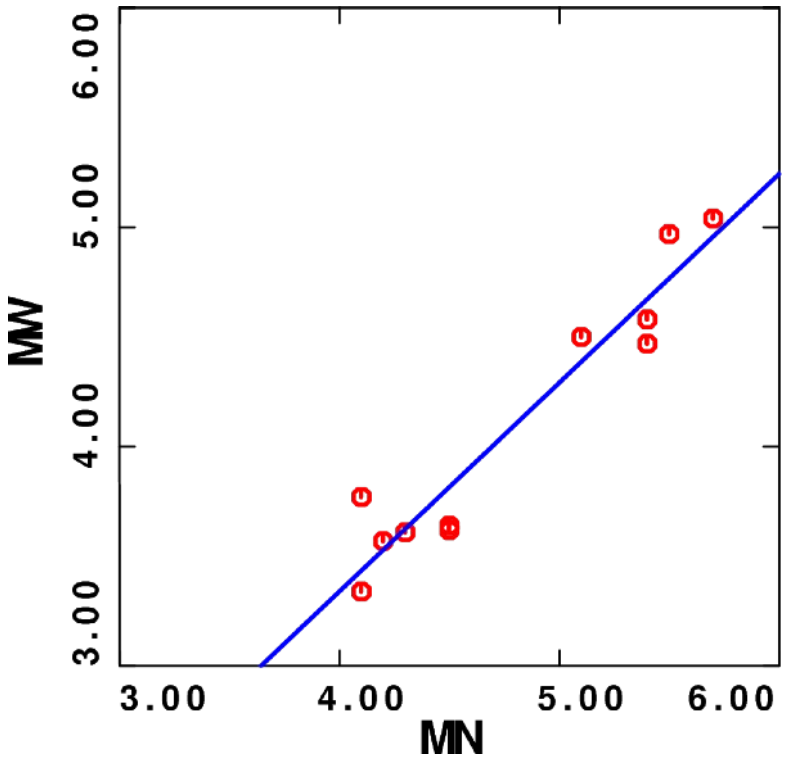

Fig. 3.3. The MW vs MN data set.

Data Processing

After downloading the waveform data in SEED format, the program *rdseed* was used to extract the traces as SAC files and the instrument response as RESP files. The program *evalresp* was used to provide tables of amplitude and phase as a function of frequency in terms of the system velocity sensitivity, e.g., counts/m/s. The sampling rate and corresponding Nyquist frequency were noted. A frequency domain deconvolution was used to yield ground velocity in m/s after applying a zero-phase bandpass filter that tapered the ground motion spectrum to zero from 1/2 the Nyquist frequency to the Nyquist frequency. The 1/2 Nyquist frequency was selected since this would ensure at least 4 points per cycle to define a sine/cosine wave.

Next the ground velocity are examined and the P- and S-wave first arrivals are selected. These instrument deconvolved traces are examined for glitches and data gaps.

The last stage is to derive ground motion parameters from each trace. Since the SLU approach (Raoof, 1999; Malagnini et al ,2000a,2000b; Malagnini and Herrmann, 2000) focuses on a complete description of the S-wave ground motion duration, peak motion and spectra are measured. Each waveform is passed through a sharp bandpass filter. We use filter center frequencies, fc, of 1, 2, 3, 4, 6, 8, 10, 12, 14 and 16 Hz. For each center frequency, the trace is high-pass filtered with an 8-pole Butterworth filter with corner frequency fc/1.414 and then low-pass filtered with an 8-pole Butterworth filter with corner frequency of 1.414 fc. The filtering is not performed unless the center frequency is less than ½ the Nyquist frequency. For each filter frequency, the duration is estimated as the time window between the 5% and 75% limits of the integrated squared velocity of the signal following the S arrival, and the Fourier velocity spectrum is obtained from the RMS spectra within the two bandpass filter corners. In addition, the spectral moments and the duration are used to estimate a predicted peak motion and corresponding confidence limits from Random Vibration Theory. Other trace parameters include the signal envelope for use in later S/N tests.

After trace parameters are determined for all traces for all events, a regression analysis is performed. The first step is to parameterize the separate peak filtered velocity and Fourier velocity data sets. This is done using a model

$$\log A = E + D + S$$

where A is either the peak filtered ground velocity (m/s) or the Fourier velocity spectra (m). D is a distance term which is forced to be 0 at a distance of 40 km. The S is a site term, which is constrained such that the sum of all vertical site terms is zero. The horizontal term is permitted to float. The distance function, D, is a piecewise linear function defined by a finite set of nodes. A differential smoothing operator is applied to the D term to yield a smooth dependence with distance. The excitation term, E, is related to the source and also actual propagation because of the constraint on the D term. For this data set, E is the level of motion at a distance of 40 km. The D term propagates that level to the the particular observation distance, and the S term permits a local site modification. The S constraint forces E to be defined as the expected network-average vertical motion at a distance of 40 km. The reasons for constraining the vertical component is due to the fact that older data sets usually consist of only vertical component data and also because the site effect of local site effects on the vertical component of the ground motion should not be as variable as for the horizontals under the assumption that the vertical motion on soft soil sites is the result of a P-wave incident at the surface because of an S-to-P conversion at the base of the sediments.

The regressions are performed using the separate peak filtered ground velocity and the Fourier velocity

spectra data sets at the individual frequencies. The purpose of this extra effort is to ultimately define a parametric model for ground motion prediction based on stochastic or random vibration theory (e.g., Boore, 2000), which requires that the model correctly match the observed Fourier spectra, peak motion and duration. This approach also recognizes the practical problems inherent in the data sets. The time-domain peak motion is the simplest to determine. The determination of the Fourier spectrum requires the specification of a signal window, the same used for the duration measurement; this is not easy to accomplish for noisy signals. However to model the observations, the prediction of peak motion takes much longer than the estimation of the spectra.

Data Quality Check

There are two ways to check the data. The first is a direct comparison to values used by Gail Atkinson (personal communication) and the other is to compare the regression results to predictions based on published models.

Comparison with Atkinson Values

In July, 2007 Gail Atkinson and I exchanged parts of our data sets. Gail Atksinson provided a subset of her data set (*gaileastz.xls)* consisting of processed values at distances of 35-45 km.

For this simple test, I focus on one event and three vertical component recordings. The tabulation here is taken from the Atkinson spreadsheet for frequencies of 4 and 10 Hz. The current SLU values are given in parentheses.

Date/Time	Mag	Lat	Lon	Sta	Comp	Log FAS 4Hz	(SLU)	Log FAS 10Hz	(SLU)
2000 2 9 23 42 2.5	MN	47.48	-69.98	A54	EHZ	-3.29	(-3.25)	-2.22	(-2.17)
2000 2 9 23 42 2.5	MN	47.48	-69.98	A21	EHZ	-3.33	(-3.28)	-2.57	(-2.63)
2000 2 9 23 42 2.5	MN	47.48	-69.98	A64	EHZ	-3.58	(-3.66)	-2.45	(-2.52)

The Atkinson values are the log10 of the Fourier acceleration in (cm/s). The SLU values have the same units and were obtained after converting from meters to cm (+2.0 $\log_{10}$ units) and from velocity to acceleration ($\log_{10} 2 \pi f$). In this simple comparison, the SLU values are about 0.05 $\log_{10}$ units greater than the Atkinson values.

Regression results and forward modeling

Because of the need to always question instrument calibration, we apply a coda normalization technique to provide an independent estimate of the spectral amplitude versus distance relation. The

coda normalization (Aki, 1980; Frankel at al, 1990) aligns the coda of all events and then plots the rescaled peak motion or Fourier velocity spectra as a function of distance. This procedure thus corrects for the source input at the given frequency and also for incorrect instrument response. It is limited by not having a time series long enough to define the coda level, especially at large distances, which is often the case with triggered data.

The peak motion or Fourier velocity spectra are then processed according to the regression equation defined above. Figure 3.4 compares the two independent estimates of the amplitude versus distance estimate at frequencies of 2 and 16 Hz. The comparison is good. The regression residual plot emphasizes that the distance range of 10 – 1000 km is well sampled. There are 2084 and 1803 observations in the 2 and 16 Hz Fourier velocity data sets. In addition, the residual plot shows no obvious distance trends.

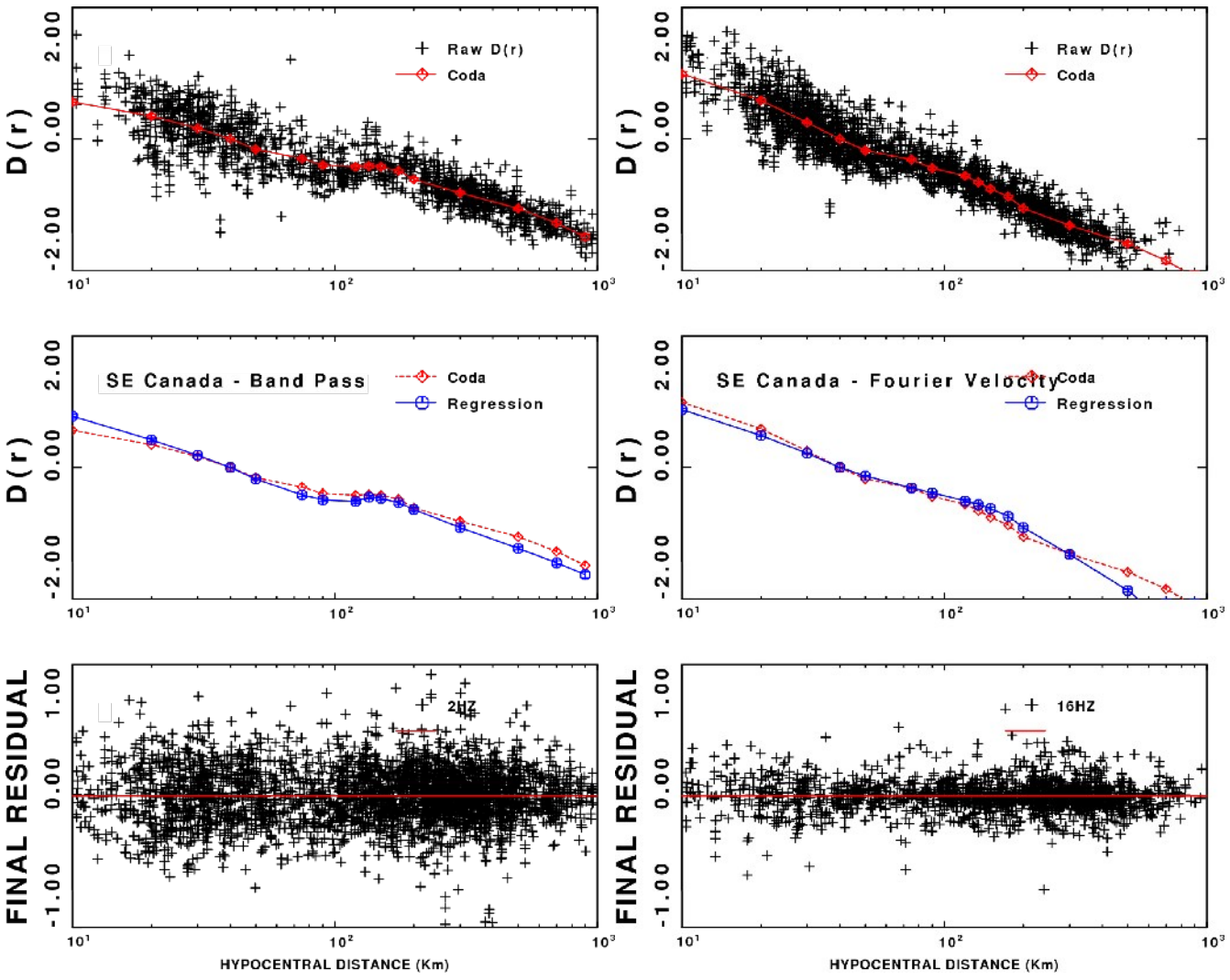

Fig. 3.4. Data set comparison for 2 Hz (left) and 16 Hz (right). Top - coda scaled amplitudes as a function of distance with a regression curve (red); Center – comparison of coda estimate (red) to the regression results (blue); Bottom – residuals from the regression analysis as a function of distance.

Forward modeling consists of defining the ground motion as a function of moment magnitude and distance. To accomplish this, we started with the SMSIM package of Boore (2002), replaced proprietary *Numerical Recipes* subroutines with open-source equivalents, and then constructed a new external wrapper so that the programs can be run using a simple control file and command line arguments. The programs are called *fscal* to predict the Fourier spectra, *tdcal* to predict peak motion in the time domain through a stochastic, filtered white noise simulation, *rvcal* to predict peak motion using random vibration theory, and *tscal* to create a simulated time series. The internal routines that compute peak motions or spectra are those of Boore (2000).

We compare the D(r) term and the E(f, 40 km) terms to predictions based on two separate models: Atkinson and Boore (1995) and Atkinson (2004), since these are the *de facto* standards for comparison. The control files used are tabulated in the Appendix of this report. Rather than plotting our D(r) term, we plot the frequency dependent residual. We present the E(f, 40 km) for events with known moment magnitude.

Fourier Velocity Data Set

Figures 3.5 and 3.6 compare show the D(r) residuals for the Atkinson and Boore (1995), AB85, and Atkinson (2004), A2004. models, respectively. The fact that the 1 Hz values are not in agreement at short distances is a problem of signal to noise as well as a problem of isolating the S-wave arrival from the P-wave at short distances, especially at low frequencies. There is also a problem at high frequencies of 12-14 Hz at large distances, which may be due to imperfect data sets, the underlying modeling assumption of a frequency independent geometrical spreading and a distance independent anelastic attenuation, or the effect is real.

In a study of the 1982 Miramichi earthquakes, Shin and Herrmann (1987) noted that at high frequencies the Lg dominates at short distances but quickly fades in the the Sn coda at large distances. If this is also seen in this data set, then the applicability of this southeastern Canada wave propagation feature to the Central and Eastern United States must be investigated. In addition, it would be very useful to investigate the significance of this effect by examining the disaggregation of seismic hazard in current models.

At short distances, e.g., 10 km, the AB95 model slightly under-predicts motions while the A2004 model over-predicts. The greatest difference between the models is seen in the 100 – 300 km distance range, at which the A2004 model over-predicts the reference distance normalized D(r), which may be due to the higher Q used in that model.

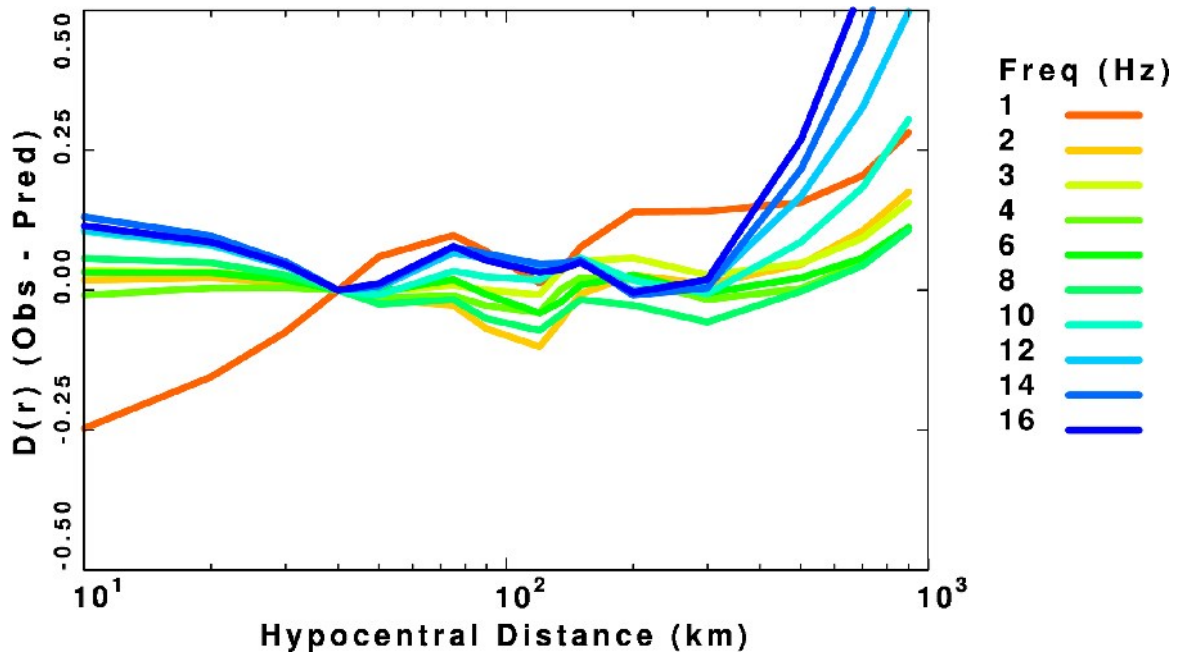

Fig. 3.5. Difference between regression D(r) and the predictions based on the Atkinson and Boore (1995) model.

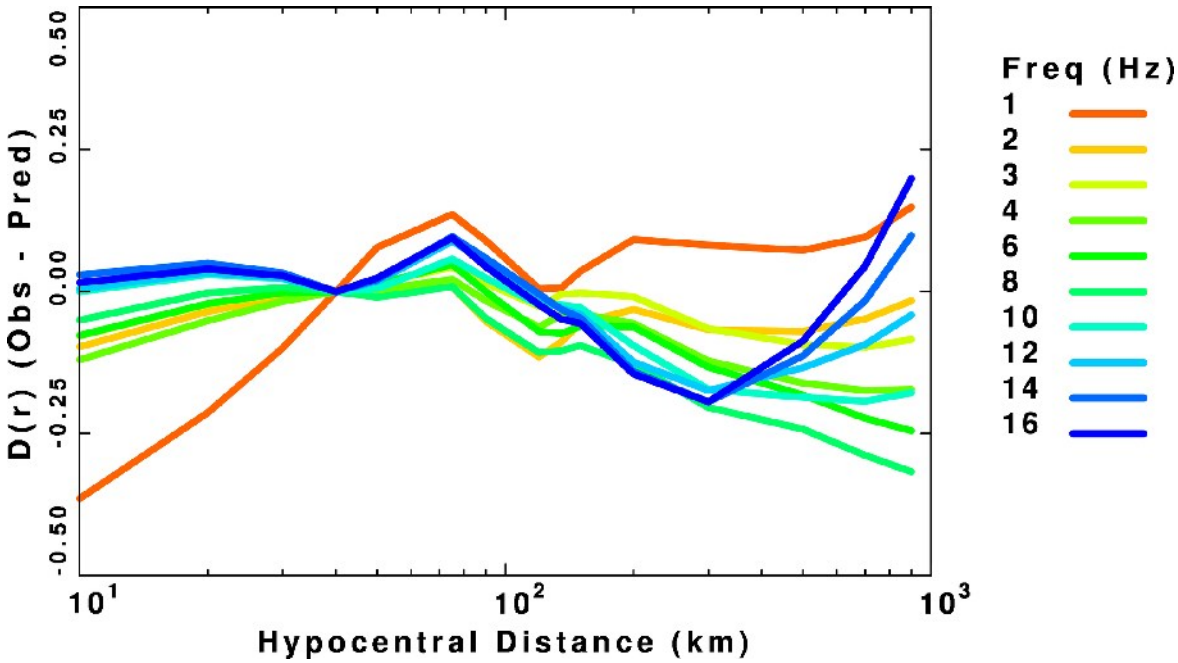

Fig. 3.6. Difference between regression D(r) and the predictions based on the Atkinson (2004) model.

Figures 3.7 and 3.8 compare the predicted and regression E(f, r=40 km) values. To obtain the predicted values, the source spectrum is defined for a given moment magnitude, which is then propagated out to a distance of 40 km, accounting for geometrical spreading and anelastic attenuation. The effect of 'kappa' and/or f_{max} is included at this point. The observed excitations are plotted for the events with know moment magnitude.

We now focus on the predictions of the two models formulated in Appendix A. For the five events with M_W near 3.5, the AB95 models may be slightly better at the lower frequencies. The difference between the two models is that the A2004 predictions are slightly lower. At the high frequencies, my implementation of the A2004 model with a fixed stress drop of 200 bars, under-predicts the observed spectra, while the AB95 model provides a reasonable fit at all frequencies.

Figure 3.9 presents the differences between observed and model predicted excitations for the two models for events with known moment magnitude. The positive residuals associated with the Atkinson (2004) model indicates that that model under-predicts the excitation.

Because we permitted the horizontal component site term to be unconstrained, we are able to compute an H/Z ratio. Figure 10 compares the H/Z ratio, with two ratios per station. For comparison Equation (8) of Atkinson (2004) is plotted.

In spite of these differences, this exercise indicates that the data set is adequate for regression analysis as part of the NGA-EAST process.

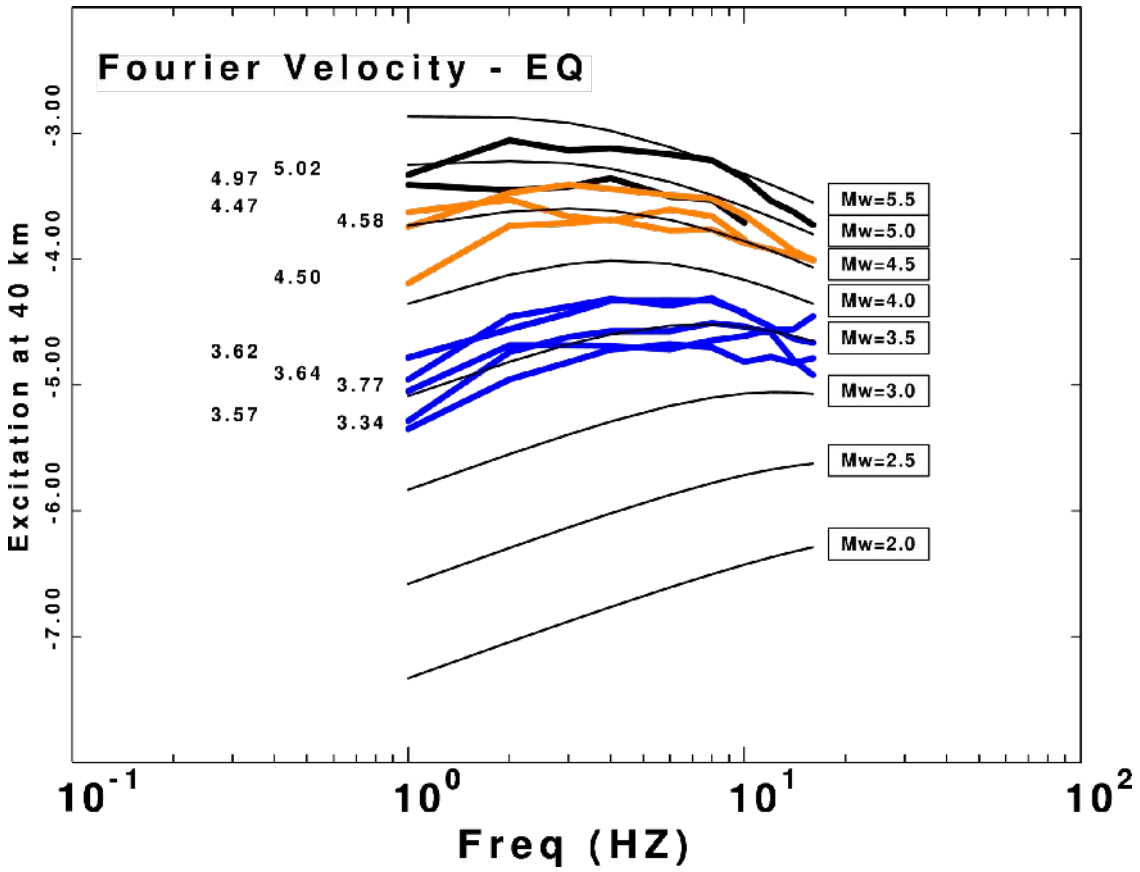

Fig. 3.7. Comparison of predicted (black) and regression determined Fourier velocity excitation (color) terms at 40 km for the Atkinson and Boore (1995) model. The predictions are annotated with the moment magnitude at the right. The moment magnitudes for the observed data at plotted at the corresponding 1 Hz levels on the left.

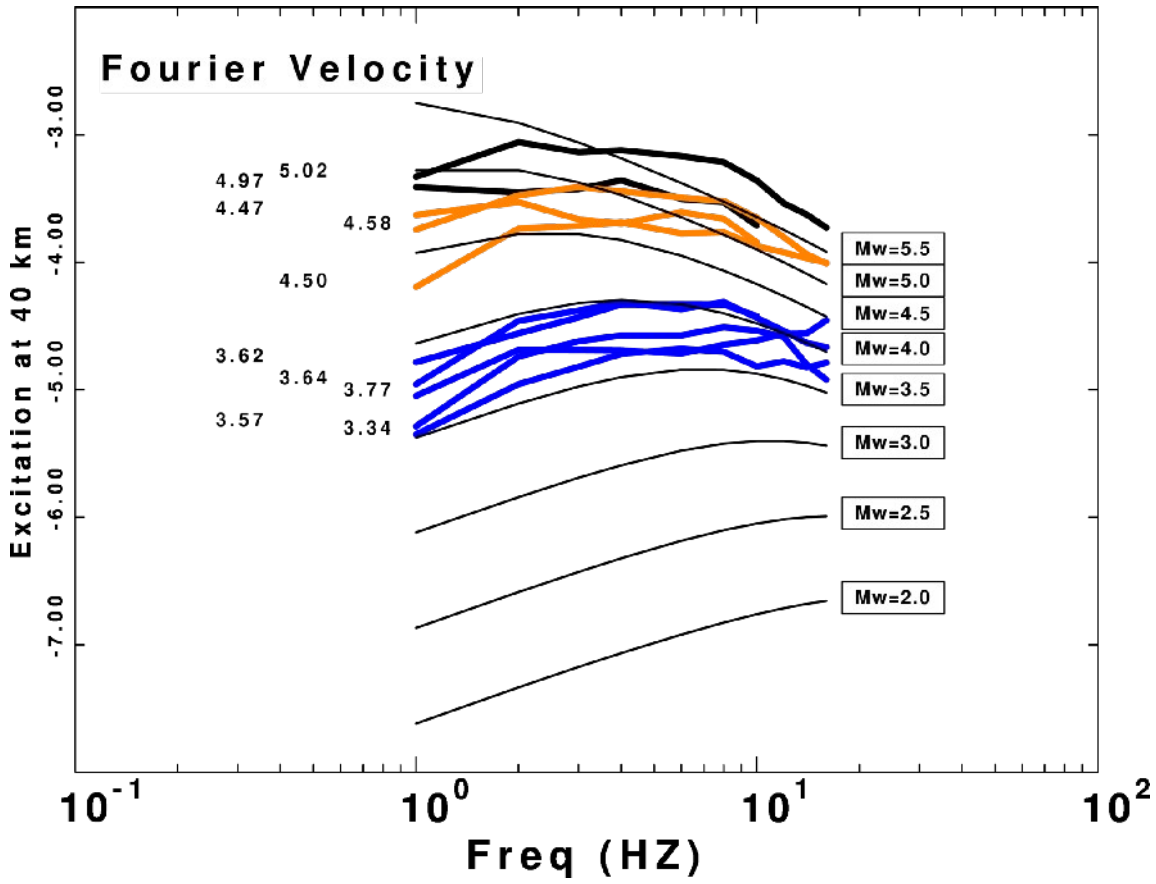

Fig. 3.8. Comparison of predicted (black) and regression determined Fourier velocity excitation (color) terms at 40 km for the Atkinson (2004) model. The predictions are annotated with the moment magnitude at the right. The moment magnitudes for the observed data at plotted at the corresponding 1 Hz levels on the left.

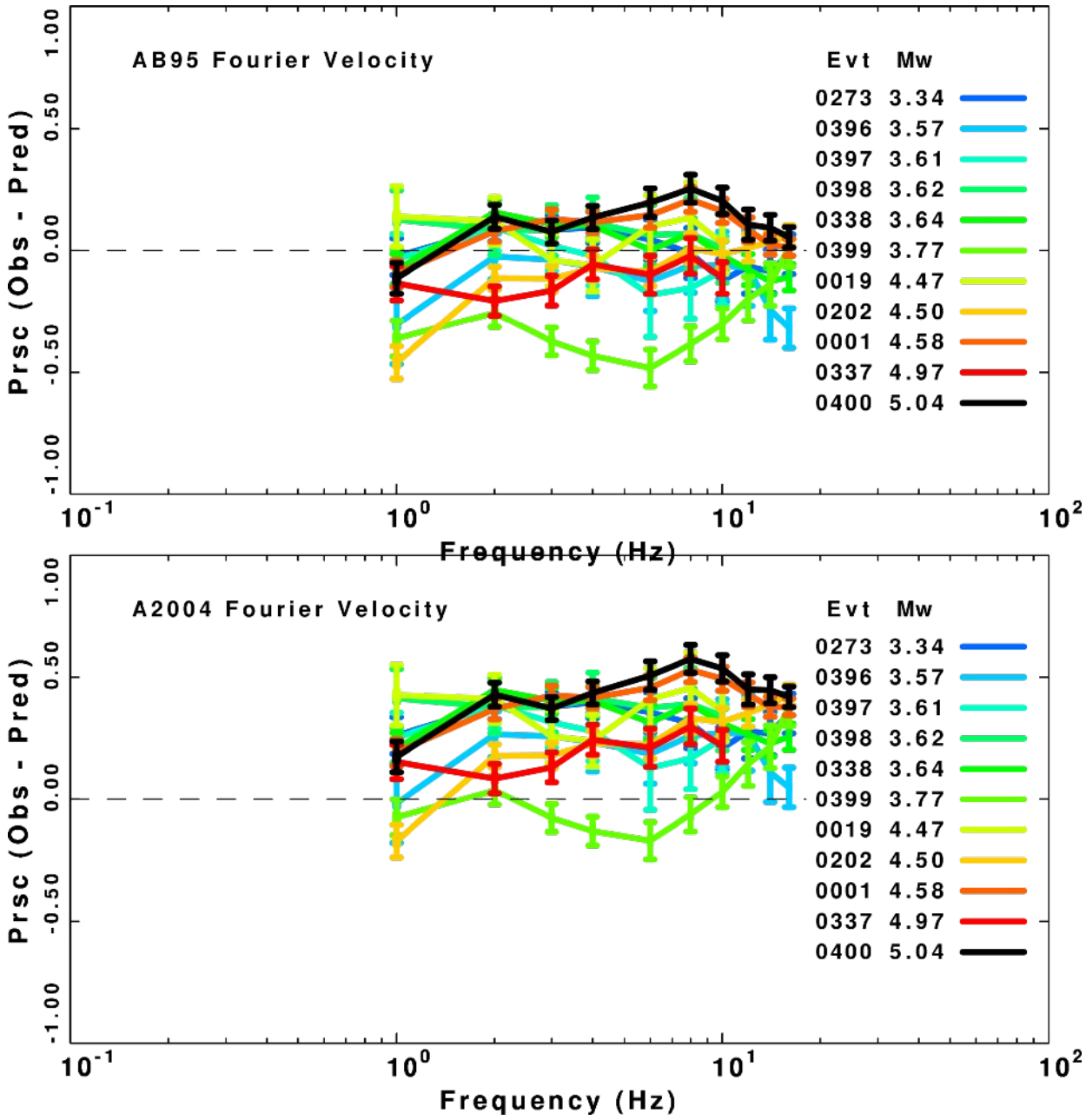

Fig. 3.9. Difference between the observed and predicted excitations for Fourier velocity at 40 km. The predictions are based on the Atkinson (2004) model with a 200 bar stress drop. The colors are keyed to the event number and the moment magnitude.

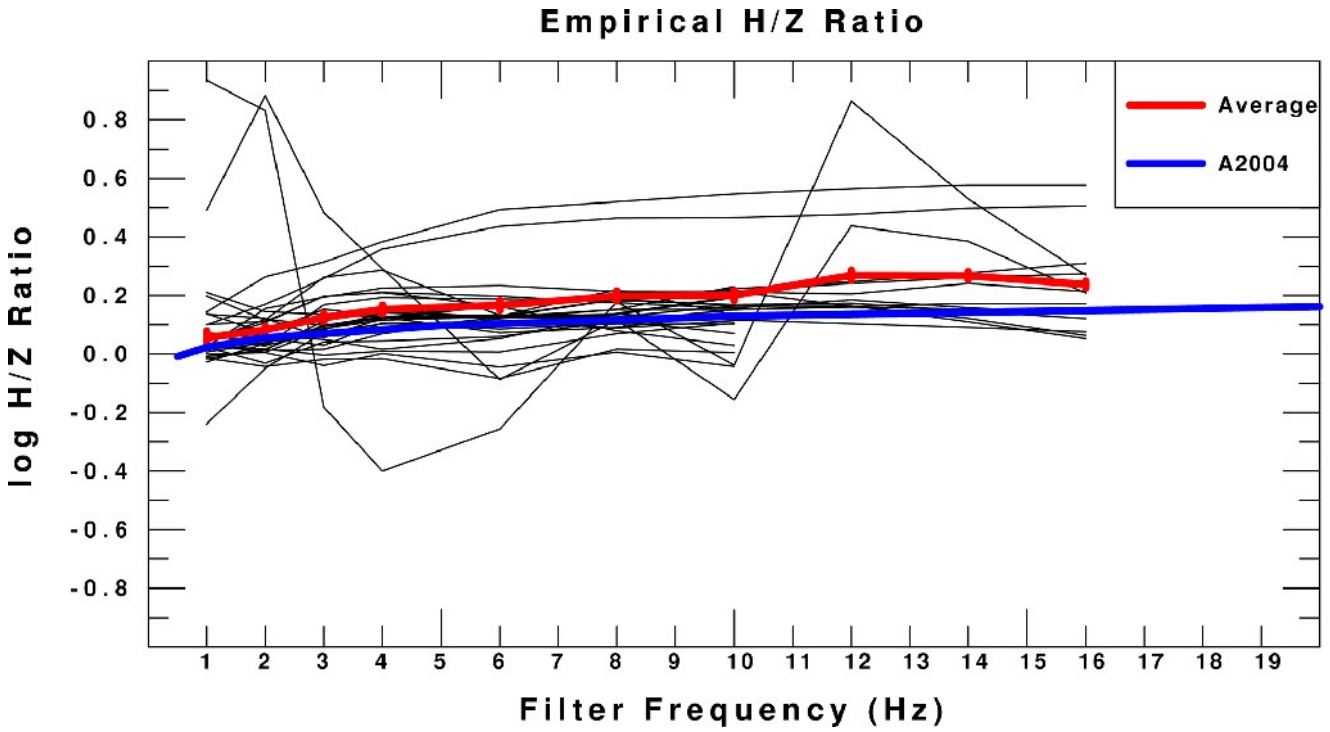

Fig. 3.10. Individual H/Z estimates (black curves) from the three-component data set of Fourier velocity. The red curve is the mean of all black curves. For reference Equation (8) of Atkinson (2004) is plotted. The large positive outliers at 2 Hz are for station PKRO. At 12 Hz the outliers are for stations A61 and PKRO.

Peak Filtered Velocity Data Set

Although not included in the current data set, it appropriate to present the a comparison of the peak filtered amplitudes. As mentioned earlier, the observed peak values are direct measurements and do not require the specification of the signal window required for the Fourier velocity spectra estimate. However, the forward prediction from the model requires a specification of the spectra and the duration. These data represent those values which have a signal-to-noise ratio ≥ 4.

Figures 3.11 and 3.12 present the difference between the D(r) from the regression and each model. Figures 3.13 and 3.14 present a comparison of the E(f, r=40 km). Figure 3.15 presents the difference between the observed and predicted excitations.

The D(r) residuals again show that the AB95 model fits better than the A2004 model at short distances. The problem for distances greater than 300 km still esists, but in the 100 – 300 km distance range, the AB95 residuals are again smaller than the A2004 model.

The comparison of the Excitation terms in Figures 3.13 and 3.14 indicate a better fit at low frequencies by the AB95 model. At high frequencies the AB95 provides a good fit, while the A2004 model again underpredicts the motions at high frequencies.

Figure 3.16 presents the H/Z ratio resulting from the regression and compares these to Equation (8) of

Atkinson (2004). Although out rations are formed from the time domain peak filtered velocity, the values are similar to those of Atkinson (2004). The error bars on our rations are not presented.

Finally Figures 3.17 and 3.18 present the duration measurements from from the traces used in the time-domain peak motion data set. There is a significant difference in the duration as a function of frequency, which is related to whether the peak motion is dominated by a single ray at or by a group of ray arrivals.

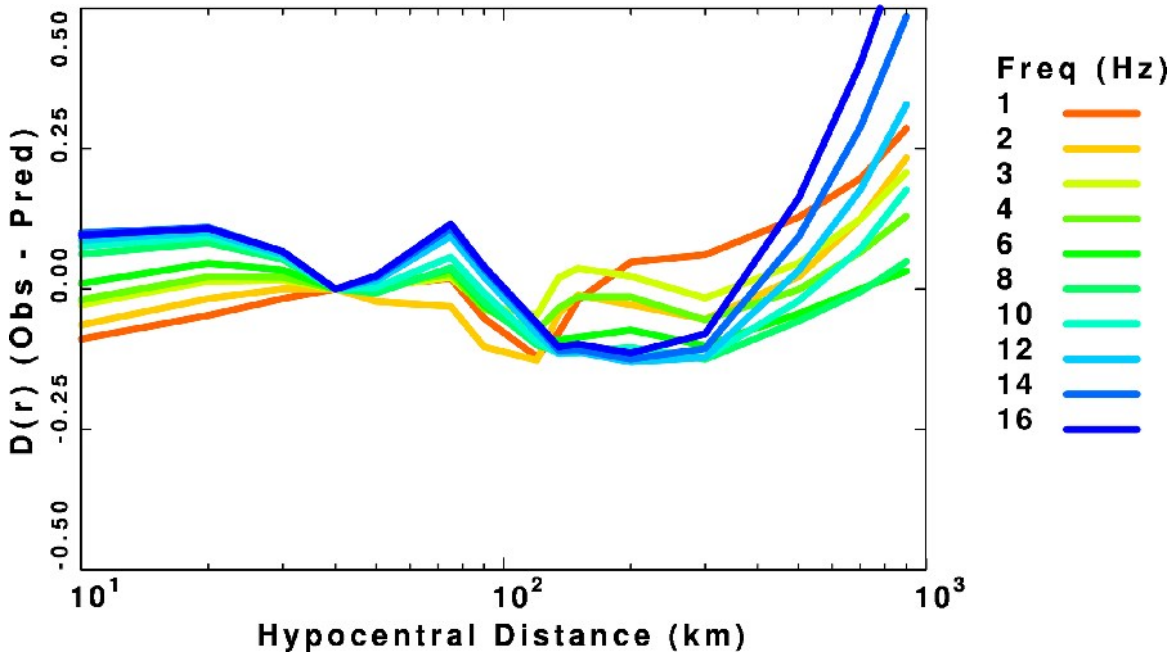

Fig. 3.11. Difference between the time-domain peak filtered velocity regression D(r) and the predictions based on the Atkinson and Boore (1995) model.

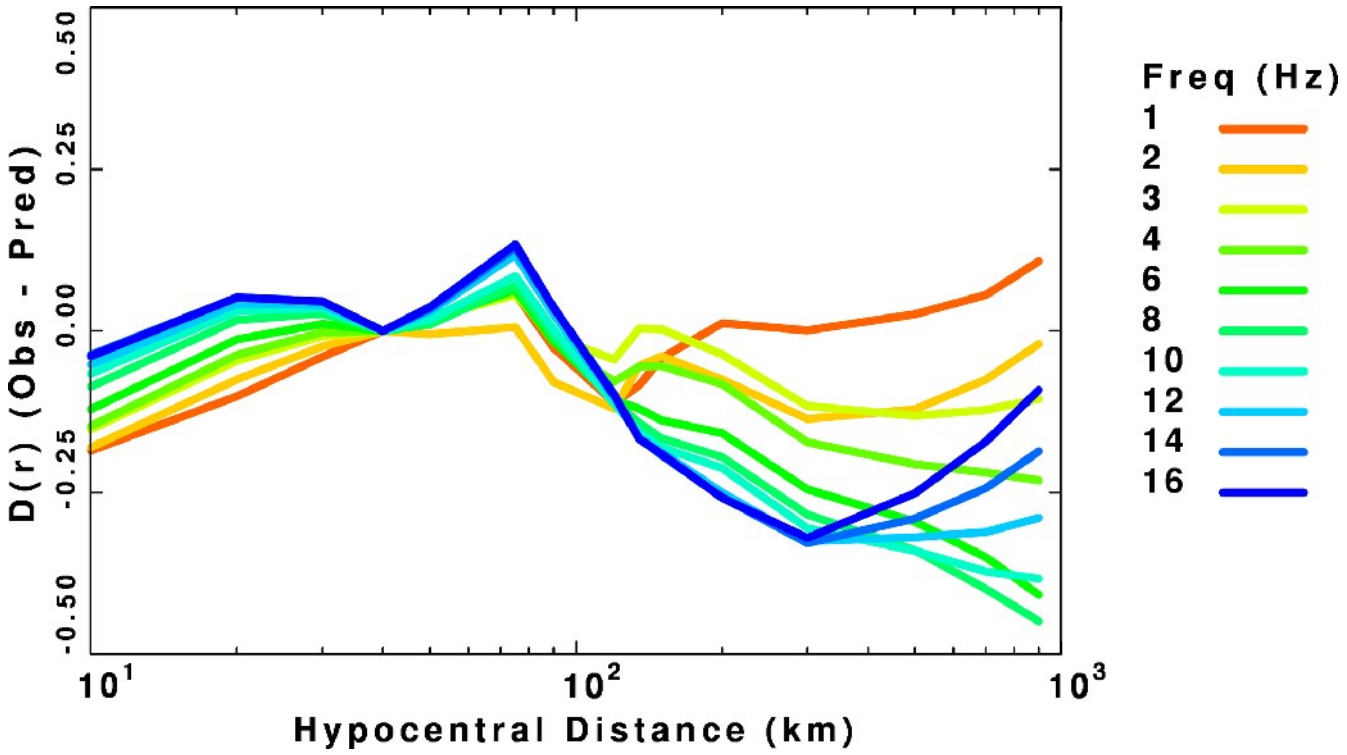

Fig. 3.12. Difference between the peak filtered velocity regression D(r) and the predictions based on the Atkinson (2004) model.

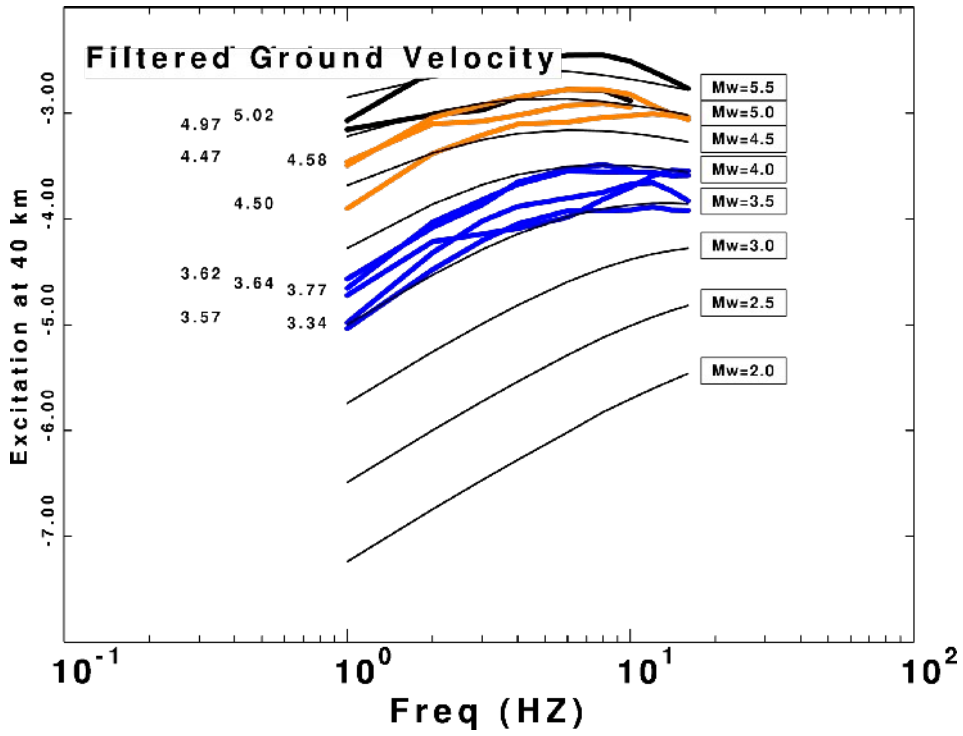

Fig. 3.13. Comparison of predicted (black) and regression determined Fourier velocity excitation (color) terms at 40 km for the Atkinson and Boore (1995) model. The predictions are annotated with the moment magnitude at the right. The moment magnitudes for the observed data at plotted at the corresponding 1 Hz levels on the left.

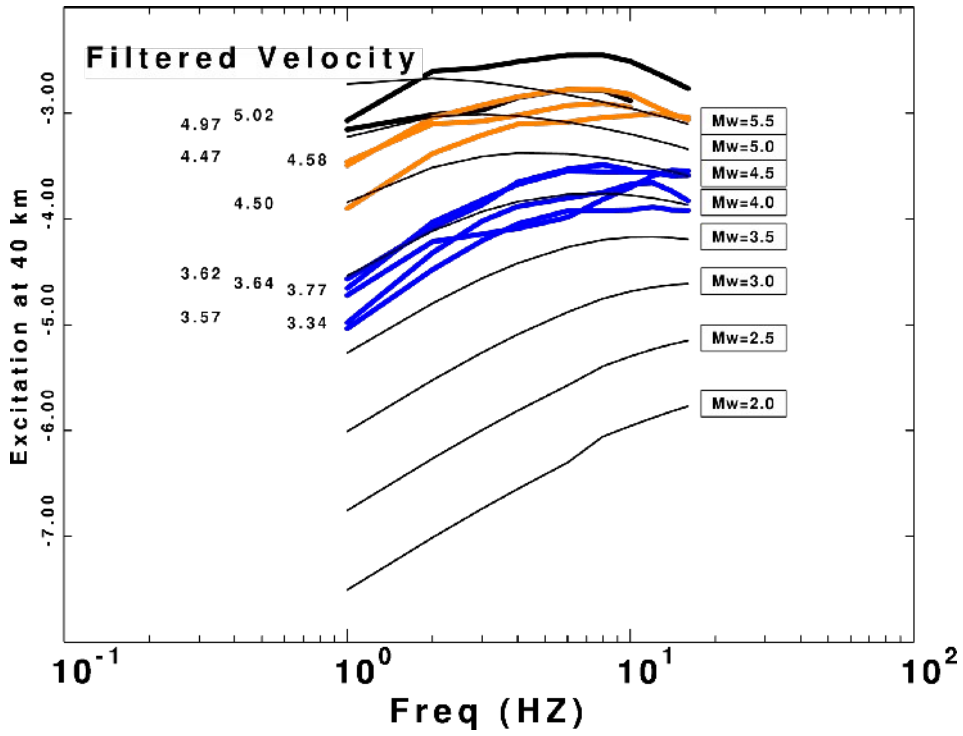

Fig. 3.14. Comparison of predicted (black) and regression determined peak filtered velocity excitation (color) terms at 40 km for the Atkinson (2004) model. The predictions are annotated with the moment magnitude at the right. The moment magnitudes for the observed data at plotted at the corresponding 1 Hz levels on the left.

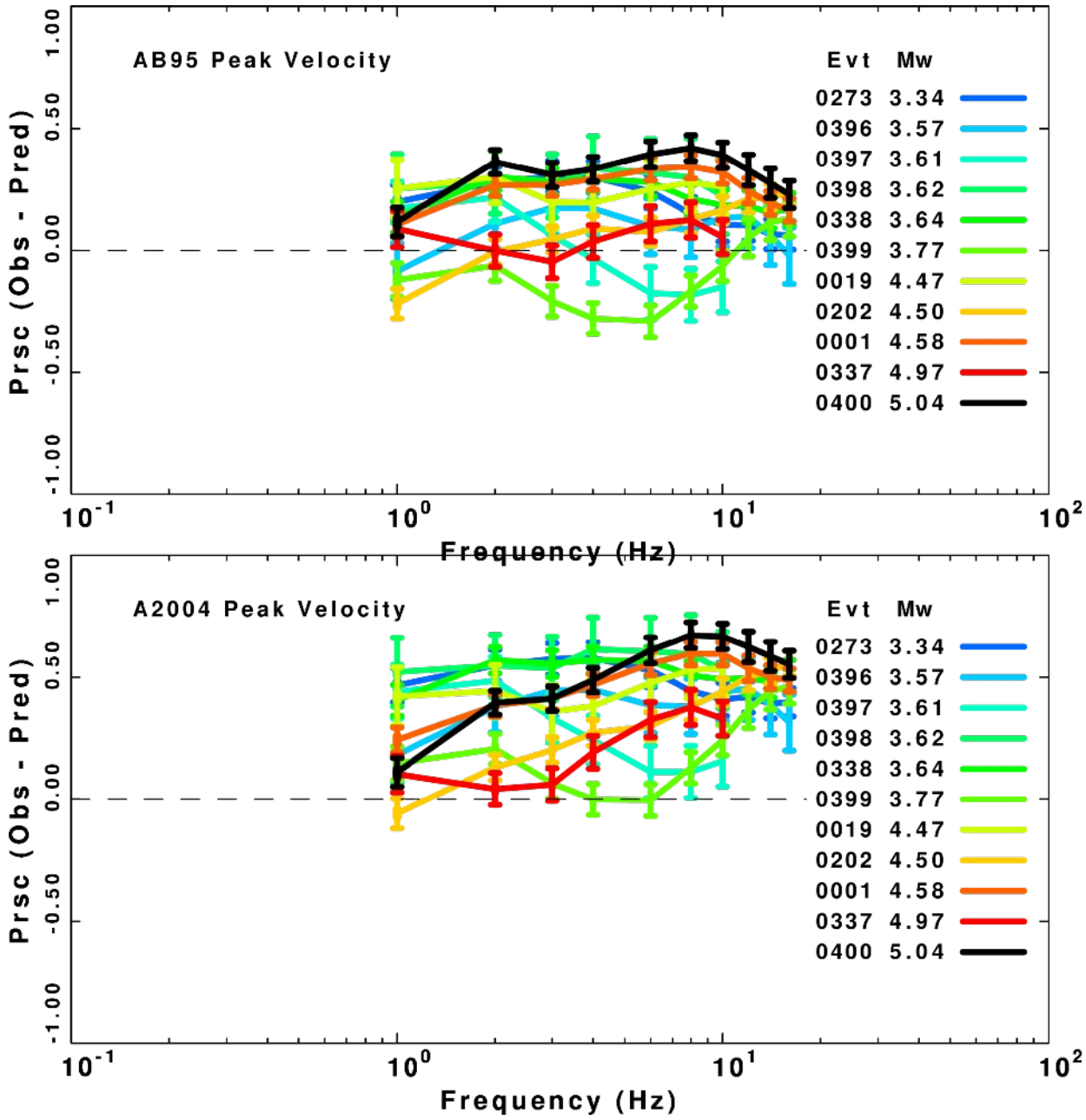

Fig. 3.15. Difference between the observed and predicted excitations for peak filtered velocity at 40 km. The predictions are based on the Atkinson (2004) model with a 200 bar stress drop. The colors are keyed to the event number and the moment magnitude.

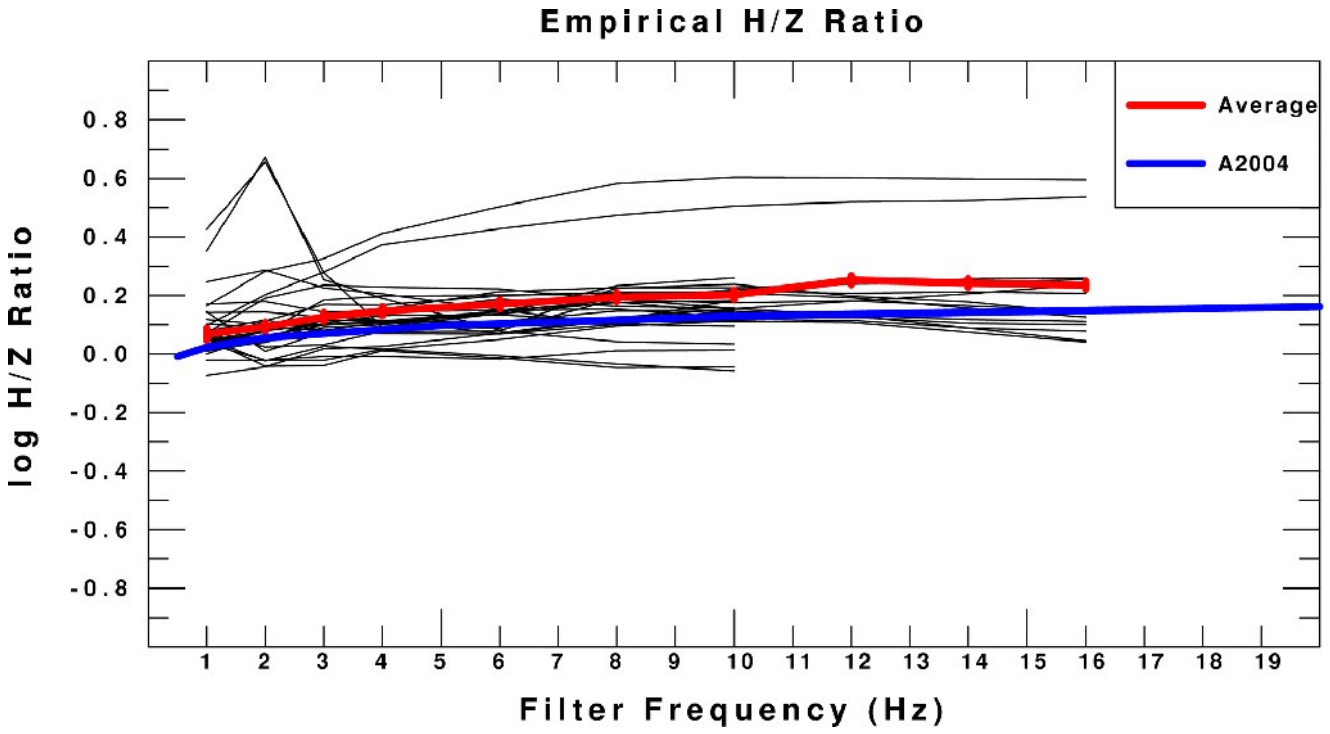

Fig. 3.16. Individual H/Z estimates (black curves) from the three-component data set of peak filtered velocity. The red curve is the mean of all black curves. For reference Equation (8) of Atkinson (2004) is plotted. The outliers at high frequency are from station A61. The outliers at a filter frequency of 2 Hz are for station PKRO.

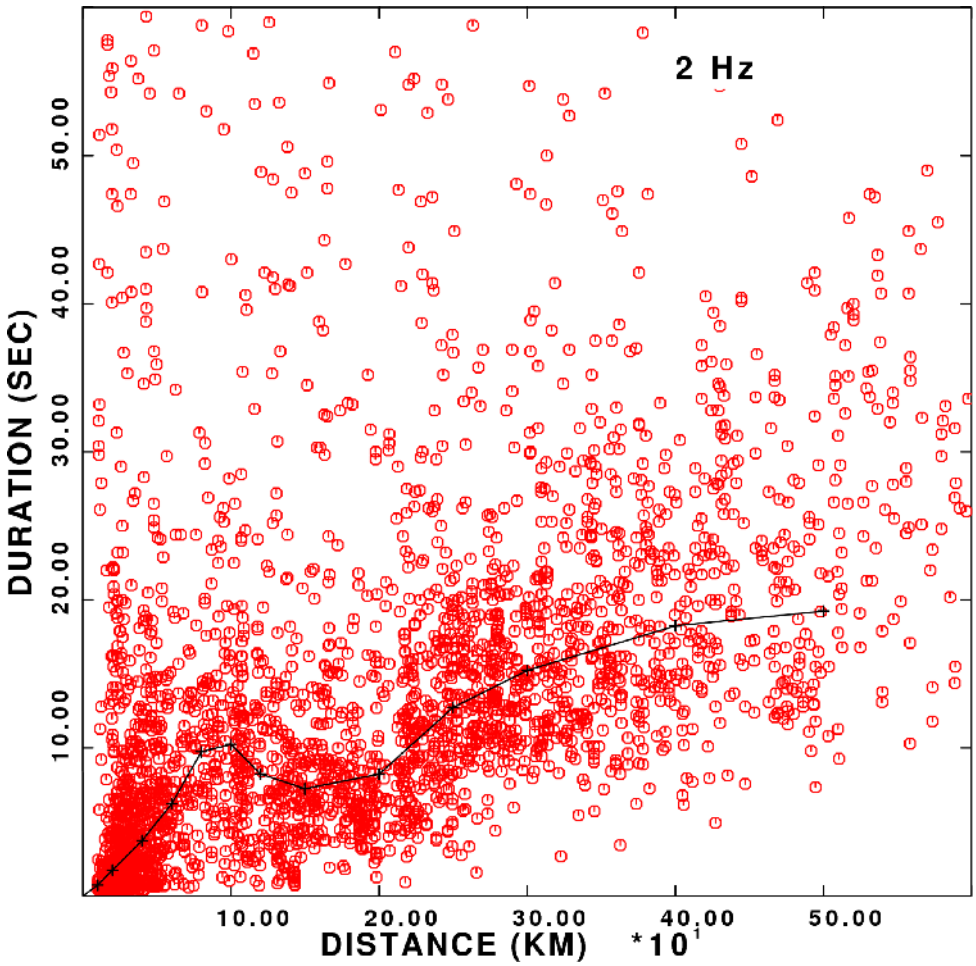

Fig. 3.17. Duration values for the 2 Hz peak velocity data set. The L-1 norm data fit is indicated by the black curve.

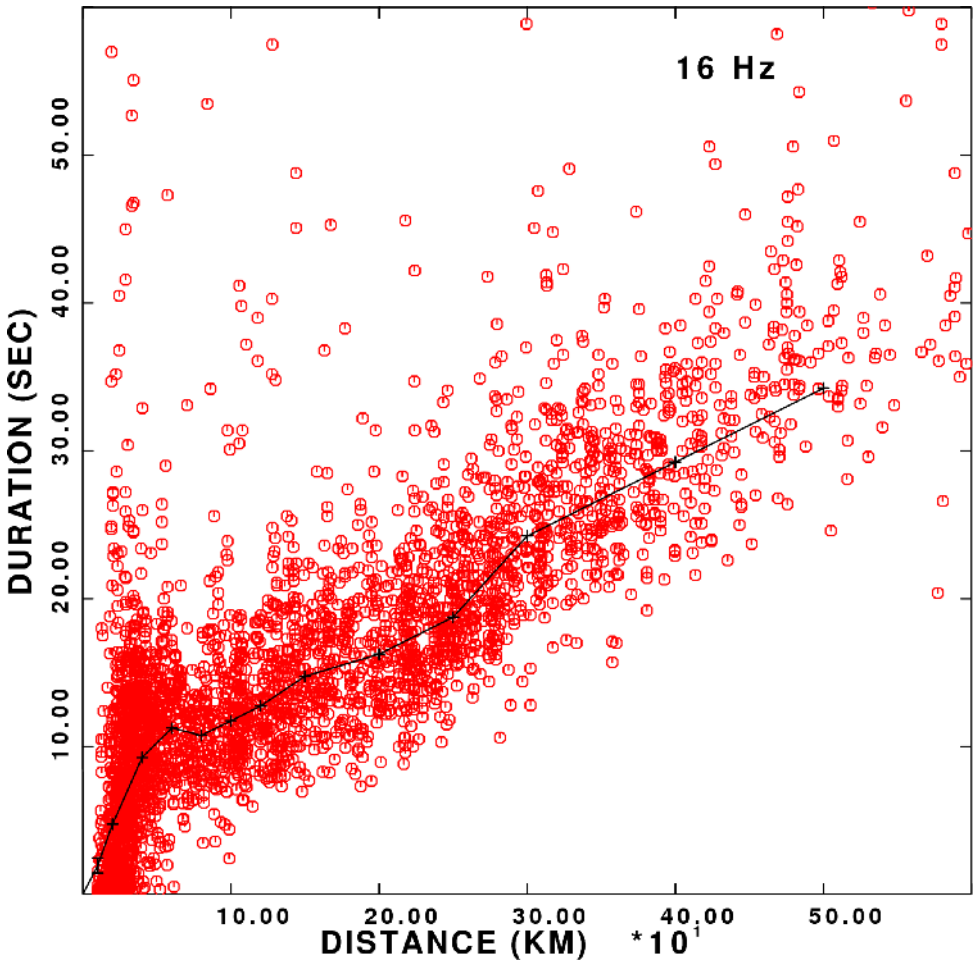

Fig. 3.18. Duration values for the 16 Hz peak velocity data set. The L-1 norm data fit is indicated by the black curve.

4. References

Aki, K. (1980). Attenuation of shear waves in the lithosphere for frequencies from 0.05 to 25 Hz, Phys. Earth Planet. Interiors 21**,** 50 –60.

Atkinson, G. M. (2004). Empirical attenuation of ground-motion spectral amplitudes int southeastern Canada and the northeastern United States, Bull. Seism. Soc. Am. 94, 1079-1095.

Atkinson, G. M., and D. M. Boore (1995). Ground-motion relations for eastern North America, Bull. Seism. Soc. Am 85, 17-30.

Boore, D.M. (2000). SMSIM – Fortran programs for simulating ground motions from earthquakes: version 2.0 — A revision of OFR 96-80-A, U.S. Geol. Surv. Open-File Rept. OF 00-509, 53 pp.

Du, W.-X., W.-Y. Kim, and L. R. Sykes (2004). Earthquake source parameters and state of stress for the northeastern United States and southeastern Canada from analysis of regional seismograms, Bull. Seism. Soc. 93, 1633-1648.

Frankel, A.., A. McGarr, J. Bicknell, J. Mori, L. Seeber and E. Cranswick (1990). Attenuation of high-frequency shear waves in the crust: Measurements from New York State, South Africa, and Southern California, J. Geophys. Res. 95, 17,441-17,457.

Malagnini, L., R. B. Herrmann, and K. Koch (2000a). Ground motion scaling in Germany, *Bull. Seism. Soc. Am*. **90,** 1052-1061.

Malagnini, L., R. B. Herrmann and M. Di Bona (2000b). Ground motion scaling in the Apennines (Italy), Bull. Seism. Soc. Am. **90,** 1062-1081.

Malagnini, L., and R. B. Herrmann (2000). Ground motion scaling in the region of the 1997 Umbria-Marche earthquake (Italy), *Bull. Seism. Soc. Am.* **90,** 1041-1051.

Mayeda, k., A. Hofstetter, J. L. O'Boyle, and W. R. Walter (2003). Stable and transportable regional magnitudes based on coda-derived moment-rate spectra, Bull. Seism. Soc. Am. 93, 224-239.

Raoof, M., R. B. Herrmann and L. Malagnini (1999). Attenuation and excitation of three-component ground motion in southern California, Bull. Seism. Soc. Am. 89, 888-902.

Shin, T.-C. and R. B. Herrmann (1987). Lg attenuation and source studies using 1982 Miramichi data, Bull. Seism. Soc. Am 77, 384-397.

5. Appendix -Ground motion forward models

The tabulations given here are the control files for defining the ground motion scaling relations. The software for computing the spectra and peak motions are available from the author.

A – Atkinson and Boore (1995) parameterization used:

This model predicts the vertical component motion for the 2-corner source model. The terminology follows that of the paper and of Boore (2000). The only difference is in the QVELOCITY field which is required to define the travel time of the signal. The SHEAR is the shear wave velocity at the source.

```
RVTDCAL1.0
COMMENT
      AB95
KAPPA
      0.000
QETA
      670     0.33
QVELOCITY
      3.8
SHEAR
      3.8
DENSITY
      2.8
DISTANCE
      3
      1.0     -1.1
      70.0    0.0
      130     -0.5
DURATION
      4
      0.0     0.0
      70.0    11.2
      130.0   7.4
      1000.0  47.40
SITE
      2
      0.0 1.0
      1000.0 1.0
FMAX
      50
BRUNE2
2
      Epsilon logfa   logfb   MWL MWU
1.00     0.000  2.678   -0.50   2.678   -0.50   -10     4
2.52          -0.637  2.41    -0.533  1.43    -0.188  4       10
```

B – Atkinson (2004) parameterization used:

This had a different distance scaling at short distances compared to the Atkinson and Boore (1995) model. Since a single source scaling model was not defined by Atkinson (2004), a 200 bar Brune model is used.

```
RVTDCAL1.0
COMMENT
      Atkinson 2004
KAPPA
      0.005
QETA
      893 0.32
QVELOCITY
      3.7
SHEAR
      3.7
DENSITY
      2.8
DISTANCE
      3
      1.0     -1.3
      70.0    0.2
      140     -0.5
DURATION
      5
      0.0     1.0
      10.0    1.0
      70.0    9.6
      130.0   7.8
      1000.0  42.6
SITE
      2
      0.0 1.0
      1000.0 1.0
PARTITION
   0.707
FREE
   2.00
RADIATION
   0.55
FMAX
      500
SIGMA
   200
```